

Effect of topographic slope on the export of nitrate in humid catchments: a 3D model study

Jie Yang¹, Qiaoyu Wang¹, Ingo Heidbüchel^{2, 4}, Chunhui Lu¹, Yueqing Xie³, Andreas Musolff², and Jan H. Fleckenstein^{2, 4}

¹State Key Laboratory of Hydrology-Water Resources and Hydraulic Engineering, Hohai University, Nanjing, China

²UFZ - Helmholtz-Centre for Environmental Research GmbH, Department of Hydrogeology, Leipzig, Germany

³School of Earth Sciences and Engineering, University of Nanjing, Nanjing, China

⁴Hydrologic Modeling Unit, Bayreuth Center of Ecology and Environmental Research (BayCEER), University of Bayreuth, Bayreuth, Germany

Correspondence to: Chunhui Lu (clu@hhu.edu.cn)

Key Points

- Young water fractions of Q and ET are correlated to topographic slope negatively and positively, respectively
- Flatter landscapes tend to retain more nitrogen mass in the soil and export less nitrogen mass to the stream
- A large young streamflow fraction is not sufficient for high in-stream nitrate concentrations.

Abstract. Excess export of nitrate to streams affects ecosystem structure and functions and has been an environmental issue attracting world-wide attention. The dynamics of catchment-scale solute export from diffuse nitrogen sources can be explained by the changes of dominant flow paths, as solute attenuation (including the degradation of nitrate) is linked to the age composition of outflow. Previous data driven studies suggested that catchment topographic slope has strong impacts on the age composition of streamflow and consequently on in-stream solute concentrations. However, the impacts have not been systematically assessed in terms of solute mass fluxes and solute concentration levels, particularly in humid catchments with strong seasonality in meteorological forcing. To fill this gap, we modeled the groundwater flow and nitrate transport for a small agricultural catchment in Central Germany. We used the fully coupled surface and subsurface numerical simulator HydroGeoSphere (HGS) to model groundwater and overland flow as well as nitrate transport. We computed the water ages using numerical tracer experiments. To represent various topographic slopes, we additionally simulated ten synthetic catchments generated by modifying the topographic slope from the real-world scenario. Results suggest a negative correlation between the young streamflow fraction and the topographic slope. This correlation is more pronounced in flat landscapes with slopes < 1:60. Flatter landscapes tend to retain more N mass in the soil (including mass degraded in soil) and export less N mass to the stream, due to reduced leaching and increased degradation. The mean in-stream nitrate concentration shows a decreasing trend in response to

35 a decreasing topographic slope, suggesting that a large young streamflow fraction is not sufficient for high in-stream
36 concentrations. Our results improve the understanding of nitrate export in response to topographic slope in a temperate
37 humid climate, with important implications for the management of stream water quality.

38

39 **Keywords:** topographic slope, coupled surface-subsurface model, young streamflow, in-stream nitrate,
40 HydroGeoSphere

41

42 **1 Introduction**

43 Globally nearly 40% of land is used for agricultural activities [Foley *et al.*, 2005], which constitutes the major source
44 of pollution with nutrients such as nitrate (referred as to N-NO₃ in this study). Excess export of nitrate to streams
45 threatens ecosystem structure and functions, as well as human health via drinking water [Vitousek *et al.*, 2009; Alvarez-
46 Cobelas *et al.*, 2008; Dupas *et al.*, 2017]. This has been an environmental issue attracting attention in Germany and
47 world-wide. The dynamics of nitrate export from diffuse nitrogen (N) sources are regulated by the dominant flow
48 paths that determine the speed at which precipitation travels through catchments before it reaches the stream [Jasechko
49 *et al.* 2016]. The process is subject to both hydrological and biogeochemical influences mediated by various factors
50 (e.g. catchment topography, aquifer properties, redox boundaries). From the perspective of sustainable intensification,
51 process understanding and assessment of potential effects of catchment topography on nitrate export are critical for
52 the management of water quality in connection with agricultural activity.

53 Field observations in central German catchments indicate that in-stream nitrate concentrations (C_Q) show significant
54 differences in mean concentrations and seasonal variations between downstream areas with gentle topography and
55 more mountainous upstream areas [Dupas *et al.*, 2017; Nguyen *et al.*, 2022]. This provides strong evidence that
56 catchment topographic slope can influence the nitrate export. In terms of water age analyses, Jasechko *et al.* [2016]
57 using oxygen isotope data from 254 watersheds worldwide showed significant negative correlation between the young
58 (age < 3 months) streamflow fraction and the mean topographic gradient. They stated that young streamflow is more
59 prevalent in flatter catchments as these catchments are characterized by shallow lateral flow, while it is less prevalent
60 in steeper mountainous catchments as these catchments promote deep vertical infiltration. This statistically significant
61 trend is consistent with the common finding that fast shallow flow paths produce young discharge and potentially
62 influence the in-stream solute concentrations [Böhlke *et al.* 2007; Benettin *et al.* 2015; Hrachowitz *et al.* 2016; Blaen
63 *et al.* 2017]. However, apart from these data-driven analyses, a more mechanistic examination/explanation with the
64 aid of fully resolved flow paths is still required. Wilusz *et al.* [2017] used a coupled rainfall-runoff and transit time
65 model to investigate the young streamflow fraction, with a focus on the effect of rainfall variability rather than on
66 topography and solute export. Zarlenga *et al.* [2022] numerically quantified the relative contributions of hillslopes and
67 the drainage network to age dynamics in streamflow, considering the influences of transmissivity and recharge,
68 without focusing on topographic slope. The effect of topographic slope on C_Q has rarely been subject to systematical
69 testing.

70 Seasonal fluctuation of C_Q is commonplace in catchments under seasonal hydrodynamic forcing. Field observations
71 in mountainous central German catchments indicate that nitrate concentrations, as well as the mass load, in streams
72 vary seasonally, with maxima during the wet winter and minima during the dry summer [Dupas et al., 2017]. Data-
73 driven analyses by Musolff et al. [2015] and Dupas et al. [2017] suggested the systematic seasonal (de)activation of
74 N source zones as an explanation for such seasonal variability. Under wetter winter conditions the near-surface N
75 source zones in agricultural soils are connected to the stream by fast shallow flow paths. Under drier summer
76 conditions those N source zones are deactivated because their direct hydrologic connectivity to the stream is replaced
77 with deeper flow paths [Dupas et al., 2017]. Based on high-frequency monitoring in the Wood Brook catchment in
78 the UK, Blaen et al. [2017] also reported mobilization of nitrate from the uppermost soil layers during high flow
79 conditions via shallow preferential flow paths, which would not occur during base flow in drier periods. This behavior
80 leads to a seasonally-variable nitrate loading due to changing flow paths and the associated variation in transit time
81 that has been observed in many catchments [Benettin et al., 2015; Hrachowitz et al., 2016; Kaandorp et al., 2018;
82 Rodriguez et al., 2018; Yang et al. 2018]. However, how this fluctuation behaves in response to catchment land surface
83 topography has not been assessed systematically yet. Such an assessment could improve our understanding of nitrate
84 export from catchments of different topographic slopes not only in terms of the mean concentration but also regarding
85 its temporal variation patterns.

86 Given that most of the above studies used data driven analysis, numerical modeling is an effective tool for the analysis
87 of water flow, age and solute transport, eliminating the need for large amounts of field data. Zarlenga and Fiori [2020]
88 presented a physically-based framework to model transient water ages at the hillslope scale, which was later used to
89 investigate the different impacts of hillslopes and the channel network on water ages in catchments [Zarlenga et al.,
90 2022]. A number studies focused on numerically simulating the nitrogen fluxes (or loads) in soil and groundwater
91 [Smith et al., 2004; Rivett et al., 2008; Lindström et al., 2010; van der Velde et al., 2012; Van Meter et al., 2017; X.
92 Yang et al., 2018, 2019; Kolbe et al., 2019; Knoll et al., 2020; Nguyen et al., 2021, 2022]. For example, van der Velde
93 et al. [2012] constructed a lumped numerical nitrate transport model for the Hupsel Brook catchment in the
94 Netherlands. Lindström et al. [2010] developed HYPE water quality model allowing for simulating the nitrogen fluxes
95 in soil. Van Meter et al. [2017] investigated the two-centuries nitrogen dynamics in the Mississippi and Susquehanna
96 River Basins using a TTD (transient time distribution) based transport approach. X. Yang et al. [2018] developed the
97 coupled mHM-Nitrate model, which can provide valuable insights into the spatial variability of water and nitrate fluxes
98 in catchment scale. Nguyen et al. [2021] further updated that model to the mHM-SAS model by implementing the
99 SAS-function based solute transport module [Harman, 2015, 2019; Rinaldo et al., 2015; van der Velde et al., 2012],
100 allowing for simulating the nitrate export from a Mesoscale Catchment. However, most of these works provided little
101 information on the spatially-explicit details (such as the flow field) for interpreting the nitrate dynamics. Physically-
102 based hydrogeological models (like, e.g., HydroGeoSphere [Therrien et al., 2010]) resolve the spatially-explicit details
103 within a catchment including the full variability of 3D flow paths in the subsurface, helping to understand the
104 seasonally changing flow patterns in response to different catchment topographies. Additionally, the widely used fully-
105 coupled surface-subsurface technology simulates the catchment as an integrated system, providing details of surface

106 water-groundwater exchanges fluxes. These details help to identify paths of rapid discharge to the land surface that
107 can considerably improve the interpretation of nitrate-export patterns.

108 Transit time distributions (TTDs) have been widely used to interpret hydrological and chemical responses in catchment
109 outfluxes – both in discharge (Q) and in evapotranspiration (ET) [Botter *et al.*, 2010, 2011; van der Velde *et al.*, 2012;
110 Heidbüchel *et al.*, 2012; Rinaldo *et al.* 2015; Harman *et al.*, 2015; 2019]. They characterize how a catchment stores,
111 mixes and releases water as well as dissolved solutes at large spatial and temporal scales [Benettin *et al.*, 2015; Harman,
112 2015; van der Velde *et al.*, 2010, 2012; Hrachowitz *et al.*, 2015; Van Meter *et al.*, 2017]. Given that the nitrate
113 attenuation is linked to the age composition of outflow, the TTDs are ideal tools for interpreting the concentration
114 dynamics with regard to catchment topographic slope. Estimating water ages in natural catchments is still a challenge
115 due to varying climate conditions, as well as the errors in algorithms (e.g. errors in the flow field during particle
116 tracking) and limited computational capacity. Yang *et al.* [2018] used particle tracking to compute the age distributions
117 in the subsurface of a study catchment (while omitting the 4% of total discharge produced by direct surface runoff and
118 ignoring the frequent exchange fluxes that may be important for solute export due to their short transit times). Zarlenga
119 *et al.*, [2022] used a physically-based semi-analytical model to compute the transient water ages in a catchment,
120 however, without considering surface runoff and hydrological losses (e.g. ET). In this study we determined the age
121 compositions of Q and ET using numerical tracer experiments, where advective-dispersive transport of the tracers was
122 solved using the fully-coupled surface-subsurface framework of HydroGeoSphere. The computed age dynamics based
123 on the tracer concentrations were representative as the tracers were able to track all the flow processes such as surface
124 runoff, groundwater flow and surface-subsurface interaction.

125 In this study, we attempted to systematically assess the effect of catchment topographic slope on the nitrate export
126 dynamics in terms of mass fluxes, concentration levels and its seasonal variability. We also seek mechanical
127 explanations for the previously found behaviors from data-driven studies (like, e.g., Jasechko *et al.* [2016]) with the
128 help of fully resolved flow paths. First, we selected a real-world small agricultural catchment ‘Schäferfetal’ in Central
129 Germany, which is characterized by strong seasonality in hydrodynamic forcing with associated shifts in the dominant
130 flow paths [Yang *et al.*, 2018]. This catchment is typical for many catchments with hilly topography under a temperate
131 humid climate. We created eleven model scenarios by adjusting the mean slope of the real-world catchment while
132 preserving the aquifer heterogeneity. Next, we modeled the water flow and nitrate transport for each catchment. The
133 flow and transport were solved using the fully coupled surface and subsurface numerical simulator HydroGeoSphere,
134 and the water ages were computed using numerical tracer experiments. Finally, the modeled flowpaths, water ages, N
135 mass fluxes and nitrate concentrations under various topographic slopes were analyzed. Through this study, we aimed
136 to (1) examine the relationship between topographic slope and N mass fluxes, and to (2) assess C_Q and its seasonal
137 variation in response to different topographic slopes.

138

139 2 Data collection

140 2.1 Real-world and synthetic catchments

141 Our study was conducted on the catchment ‘Schäfertal’, situated in the lower part of the Harz Mountains, Central
142 Germany (Figure 1a). The catchment has an area of 1.44 km². The hillslopes are mostly used for intensive agriculture
143 while the valley bottom contains riparian zones with pasture and a small stream draining the water out of the catchment.
144 The gauging station at the outlet of the catchment provides Q records. This gauging station is the only outlet for
145 discharging water from the catchment, because a subsurface wall was erected underneath the gauging station across
146 the valley to block subsurface flow out of the catchment. A meteorological station 200 m from the catchment outlet
147 provides records of precipitation (J), air and soil temperatures, radiation and wind speed. The modeled catchment has
148 a mean topographic slope of ~1:20, estimated using a cross-section perpendicular to the stream (Figure 1a). The aquifer
149 thickness varies from ~5 m near the valley bottom to ~2 m at the top of the hillslope. Groundwater storage is low
150 (~500 mm) in such a thin aquifer and mostly limited to the vicinity of the channel with the upper part of the hillslopes
151 generally unsaturated. The stream bed has a depth of 1.5 m below the land surface. Aquifer properties (e.g. hydraulic
152 conductivity) change from the hillslope, dominated by Luvisols and Cambisols, to the valley bottom, dominated by
153 Gleysols and Luvisols [Anis and Rode, 2015]. Apart from that, the aquifer generally consists of two layers: the top
154 layer of approximately 0.5 m thickness with higher porosity and a developed root zone from crops, and the base layer
155 with smaller porosity due to high loam content [Yang *et al.*, 2018]. Subsequently, ten property zones were used (Figure
156 1b), with zonal parameter values following the model in Yang *et al.*, [2018] listed in Table 1.

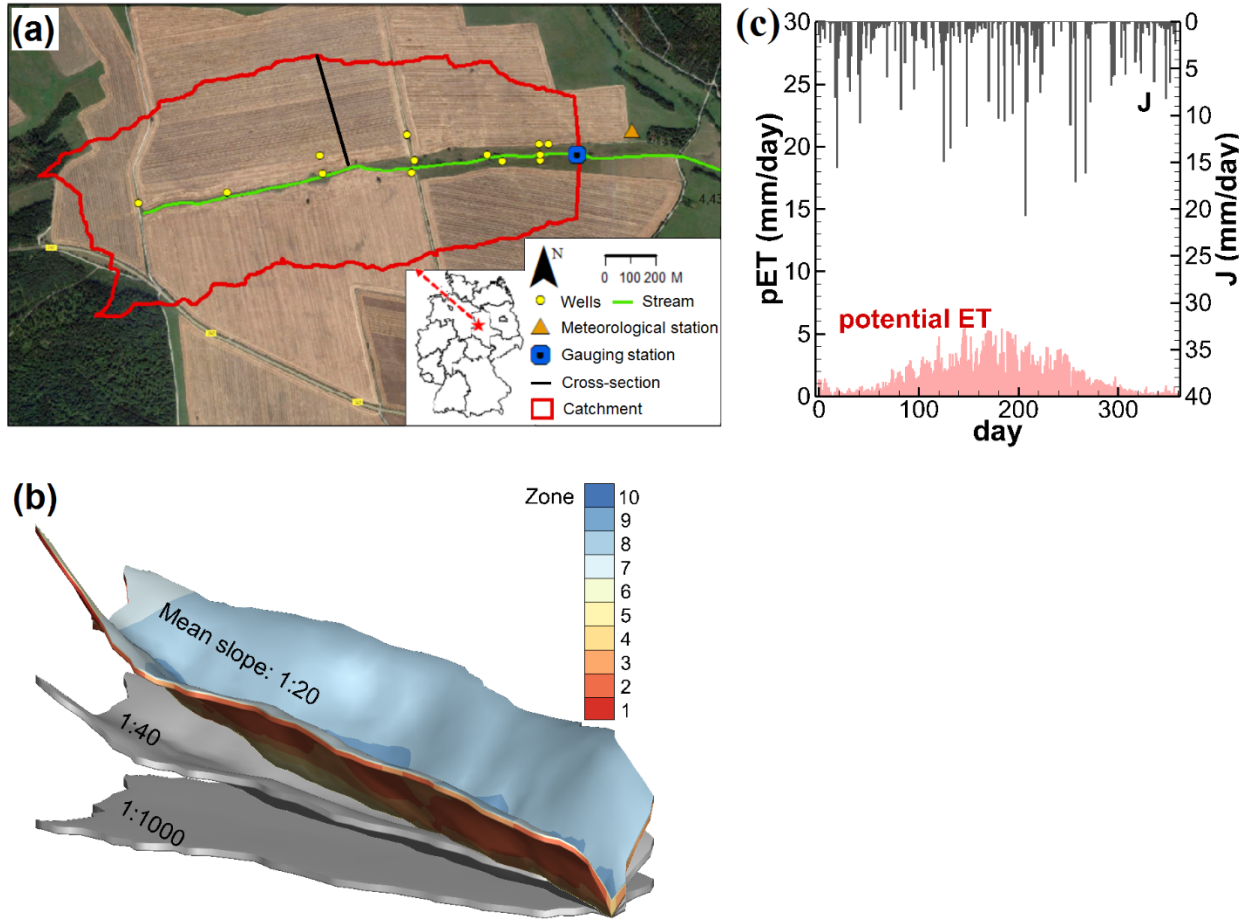
157 Based on this real-world catchment, ten synthetic catchments were generated by adjusting elevations (land surface
158 and aquifer bottom), such that the mean topographic slope ranges from 1:20 (steep) to 1:22, 1:25, 1:30, 1:40, 1:60,
159 1:80, 1:100, 1:200, 1:500 and 1:1000 (flat, Figure 1b). The aquifer depth and heterogeneity were preserved during the
160 adjustments. In total, eleven catchments were used for flow and transport simulations. The catchment with the original
161 topography (1:20) is selected as the base scenario.

162

163 2.2 Climate

164 The considered climate for the catchments was derived from the catchment ‘Schäfertal’ located in a region with
165 temperate humid climate and pronounced seasonality. According to the meteorological data records from 1997 to
166 2007, the mean annual J and Q (per unit area) are 610 mm and 160 mm, respectively. Actual mean annual ET based
167 on the ten-year water balance ($J = ET + Q$) is 450 mm. Mean annual potential ET is 630 mm [Yang *et al.*, 2018]. The
168 humid climate is representative for wet regions, quantified by an aridity index ($J / \text{potential ET}$ [Li *et al.*, 2019]) of
169 1.0. The ET is the main driver of the hydrologic seasonality as the precipitation is more uniformly distributed across
170 the year (Figure 1c).

171



172 **Figure 1.** (a) The catchment ‘Schäferfalter’, Central Germany (background image from © Google Maps). (b) The
 173 catchments with mean topographic slopes of 1:20, 1:40 and 1:1000. (c) The measured precipitation J and the
 174 estimated potential evapotranspiration ET for the year 2005 under the humid climate [Yang *et al.*, 2018]. Ten aquifer
 175 property zones in (b) were defined in the subsurface of the catchment for zonal parameter values (e.g. hydraulic
 176 conductivity).
 177

178

179 3 Methods

180 3.1 Flow and nitrate transport

181 *Flow model*

182 It is necessary to solve both groundwater and surface water flow because the spatially-explicit details in the catchment
 183 including the specific flow paths and exchange fluxes are necessary to interpret the effect of varying topographic slope
 184 on nitrate transport. We simulated the flow system using the fully coupled surface and subsurface numerical model
 185 HydroGeoSphere, which solves for variably saturated groundwater flow with the Richards’ equation and for surface
 186 flow with the diffusion-wave approximation of the Saint-Venant equations [Therrien *et al.*, 2010]. Additionally, the
 187 exchange flux between groundwater and surface water can be implicitly simulated. The nitrate transport is simulated

188 in the groundwater flow, surface flow and exchanges fluxes by solving the advection-dispersion-diffusion equation
189 describing the conservation of nitrate mass. HydroGeoSphere has been successfully used to simulate catchment
190 hydrological processes and solute transport in many studies [e.g. Therrien *et al.*, 2010; Yang *et al.*, 2018], therefore
191 governing equations and technical details are not explicitly repeated here.

192 In our previous work Yang *et al.* [2018], a hydrological flow model has already been established for the catchment
193 ‘Schäferfetal’. It was calibrated against measured groundwater levels and stream discharge Q. The optimized parameter
194 values are listed in Table 1. In this work, we performed our simulations based on that flow model, with the nitrate
195 transport process being added while maintaining the model setup. We provide a brief review of that flow model here.
196 Readers may refer to Yang *et al.* [2018] for a full description of the model and its calibration.

197 The modeled subsurface of the catchments was discretized into 9 horizontal layers between the land surface and the
198 aquifer base, with thinner layers in the upper part (0.1 m) to better represent the unsaturated zone and compute the ET.
199 In total, the subsurface was discretized by a mesh of 13860 prisms, with the horizontal size of the prisms ranging from
200 30 to 50 m. The topmost 1540 triangles were used to discretize the surface domain, where surface flow was simulated.
201 Ten property zones for the subsurface were defined (Figure 1b), being assigned with the zonal hydraulic conductivity
202 and porosity values (Table 1). ET was simulated as a combination of plant transpiration from the root zone (top 0.5 m
203 soil) and evaporation down to the evaporation depth (0.5 m), which are both constrained by soil water saturation.
204 Regarding the flow boundary conditions, spatially uniform and temporally variable J was applied to the land surface.
205 Spatially constant and temporally variable potential ET was applied to the aquifer top to calculate the actual ET. The
206 bottom of the aquifer was considered an impermeable boundary. A critical depth boundary condition was assigned to
207 the catchment outlet to simulate the stream discharge Q, which was compared to the measured Q during the calibration.
208 The software PEST [Doherty and Hunt, 2010] was used for the transient calibration. After calibration, the time-
209 variable groundwater levels were well replicated by the flow model for most of the wells, with mean coefficients of
210 determination (R^2) of 0.43. The fit between the simulated and measured Q was satisfactory with a R^2 of 0.61. The
211 calibrated model successfully simulated the flow system from 1997 to 2007.

212 In this study, we continued to use the above-described model setup, including the mesh, the parameters and the flow
213 boundary conditions, for the eleven catchments with different topography. Note that the mesh was adapted to the
214 change of the topography by changing node elevations vertically. However, to simplify the flow simulation and the
215 age computation (described in section 3.2), we selected the year 2005 as a representative year and assumed that all the
216 years have the identical climate (J and potential ET) as the year 2005. Therefore, J and potential ET of 2005 (Figure
217 1c) were cycled and applied to the catchments for all the simulated years.

218

219 **Table 1.** The key flow parameters and their values following *Yang et al.*, [2018].

Parameter	Process	Type	Value
Hydraulic conductivity	Subsurface	zonal	Zonal values (range [$3.6 \cdot 10^{-5}$ - 2.0] m day ⁻¹)
Porosity	Subsurface	zonal	Zonal values (range [0.01 - 0.35])
Residual saturation	Subsurface	uniform	0.08 [-]
Inverse of air entry pressure α	Subsurface	uniform	3.6 m^{-1}
Pore-size distribution index β	Subsurface	uniform	2 [-]
Manning roughness coefficient	Surface	uniform	$6.34 \cdot 10^{-6} \text{ day m}^{-1/3}$
Longitudinal dispersivity	Transport	uniform	8 m
Lateral and vertical dispersivity	Transport	uniform	0.8 m
Molecular diffusion coefficient	Transport	uniform	$10^{-9} \text{ m}^2 \text{ s}^{-1}$
Degradation coefficient	Transport	uniform	0.009 day^{-1}
Transpiration fitting parameters:			
C1	ET	uniform	0.17 [-]
C2	ET	uniform	0.00 [-]
C3	ET	uniform	3.00 [-]
Transpiration limiting saturations:			
Wilting point	ET	uniform	0.1 [-]
Field capacity	ET	uniform	0.2 [-]
Oxic limit	ET	uniform	0.9 [-]
Anoxic limit	ET	uniform	1.0 [-]
Evaporation limiting saturations:			
Minimum	ET	uniform	0.1 [-]
Maximum	ET	uniform	0.2 [-]

220

221

222

223 ***Transport boundary conditions and parameters***

224 The nitrogen (N) pool is formed in the soil zone of the catchments, representing a nitrate source zone. The N pool is
 225 controlled by various complex processes. It is replenished by external inputs from atmospheric deposition, biological
 226 fixation, animal manure from the pasture area, and fertilizer from the farmland on the hillslopes. Nitrate that can be
 227 transported with water is formed and leached from this N pool by a microbiological immobile-mobile exchange
 228 process [*Musolff et al.*, 2017; *Van Meter et al.*, 2017]. In our study, we employed the simplified framework by *Yang*
 229 *et al.*, [2021] to track the fate of N in the N pool (Figure 2a). This framework was derived from the ELEMNT
 230 approach (Exploration of Long-tErM Nutrient Trajectories, *Van Meter et al.*, 2017), which uses a parsimonious
 231 modeling framework to estimate the biogeochemical legacy nitrate loading in the N pool and the N fluxes leaching
 232 from the N pool to the groundwater. This framework assumes that total N load in the N pool is comprised by inorganic
 233 N (SIN) and organic N (SON). Two types of SON are distinguished: active organic N (SON_a) with faster reaction
 234 kinetics and protected organic N (SON_p) with slower reaction kinetics. It is assumed that the external N input
 235 contributes only to the SON. The SON is mineralized into SIN. The SIN is further consumed by plant uptake and

236 denitrification, and finally leaches to groundwater as dissolved inorganic N (DIN, representing mainly nitrate in the
 237 studied catchment [Yang *et al.*, 2018; Nguyen *et al.*, 2021]). The framework is acceptable due to the fact that most of
 238 the nitrate fluxes from source zones has undergone biogeochemical transformation in the organic N pool [Haag and
 239 Kaupenjohann, 2001]. The framework simplifies complexities of different N pools and transformations via
 240 mineralization, dissolution, and denitrification within the soil zone [Lindström *et al.*, 2010], while preserving the main
 241 pathway for nitrate leachate.

242 The governing equations to calculate these N fluxes follow the ones in Yang *et al.*, [2021]. A specific portion (h) of
 243 the external N input contributes to the SON_p pool, and the rest contributes to the SON_a pool. The portion h is the land-
 244 use dependent protection coefficient [Van Meter *et al.*, 2017]. The mineralization and denitrification are described as
 245 first order processes with rate coefficients k_a , k_p , and λ_s respectively, using:

$$246 \quad MINE_a = k_a \cdot f(temp) \cdot SON_a \quad (1)$$

$$247 \quad MINE_p = k_p \cdot f(temp) \cdot SON_p \quad (2)$$

$$248 \quad DENI_s = \lambda_s \cdot SIN \quad (3)$$

249 where $MINE_a$, $MINE_p$, $DENI_s$ ($\text{kg ha}^{-1} \text{ day}^{-1}$) are the mineralization rates for SON_a and SON_p , and denitrification rate
 250 for SIN . k_a , k_p , and λ_s (day^{-1}) are coefficients for the first order processes. $f(temp)$ is a factor representing a constraint
 251 by soil temperature [Lindström *et al.*, 2010]. Note that the mineralization and plant uptake occur in the N pool.
 252 Denitrification can occur in both the N pool and later in groundwater. The plant uptake rate UPT follows the equation
 253 used in the HYPE model [Lindström *et al.*, 2010]:

$$254 \quad UPT = \min(UPT_p, 0.8 \cdot SIN) \quad (4)$$

$$255 \quad UPT_p = p1/p3 \cdot \left(\frac{p1-p2}{p2}\right) \cdot e^{-(DNO-p4)/p3} / \left(1 + \left(\frac{p1-p2}{p2}\right) \cdot e^{-(DNO-p4)/p3}\right)^2 \quad (5)$$

256 where UPT and UPT_p ($\text{kg day}^{-1} \text{ ha}^{-1}$) are the actual and potential uptake rates. The computation of UPT_p considers a
 257 logistic plant growth function. DNO is the day number. $p1$, $p2$, $p3$ are three parameters depending on the crop/plant
 258 type, they are in the units of (kg ha^{-1}), (kg ha^{-1}), and (day), respectively. $p4$ is the day number of the sowing date. The
 259 leaching process allows for SIN to leach from the soil (N pool) to the groundwater. The leaching rate LEA (kg ha^{-1}
 260 day^{-1}) is defined as a first order process as:

$$261 \quad LEA = f \cdot SIN / \Delta t \quad (6)$$

$$262 \quad f = (1 - \exp^{-a \frac{wal}{\theta d}}) \quad (7)$$

$$263 \quad wal = q \cdot \Delta t \quad (8)$$

264 where f is a factor, ranging between [0, 1], to determine the portion of SIN that leaches into groundwater during a time
 265 step Δt . a is unit-less leaching factor. θ is the soil porosity. d is the soil depth. wal [L] is the water available for
 266 leaching during Δt . wal can be estimated using the Darcy fluxes q [LT^{-1}], which are provided by the flow simulations
 267 for each cell of the mesh. Physically, f is a function of the ratio between wal and the volume of soil voids $\theta \cdot d$,
 268 representing the ability of water to flush the SIN . This formulation of LEA is modified from the ones used in Pierce
 269 *et al.*, [1991], Shaffer *et al.* [1991] and Wijayantiati *et al.* [2017], to comply with the spatially-distributed
 270 HydroGeoSphere model.

271 **Table 2.** The parameters for the N pool and nitrate transport. The parameters with a range are calibrated. The
 272 adjustable ranges are selected to cover the values that the parameters can potentially take on or the values reported
 273 by the referred literature.

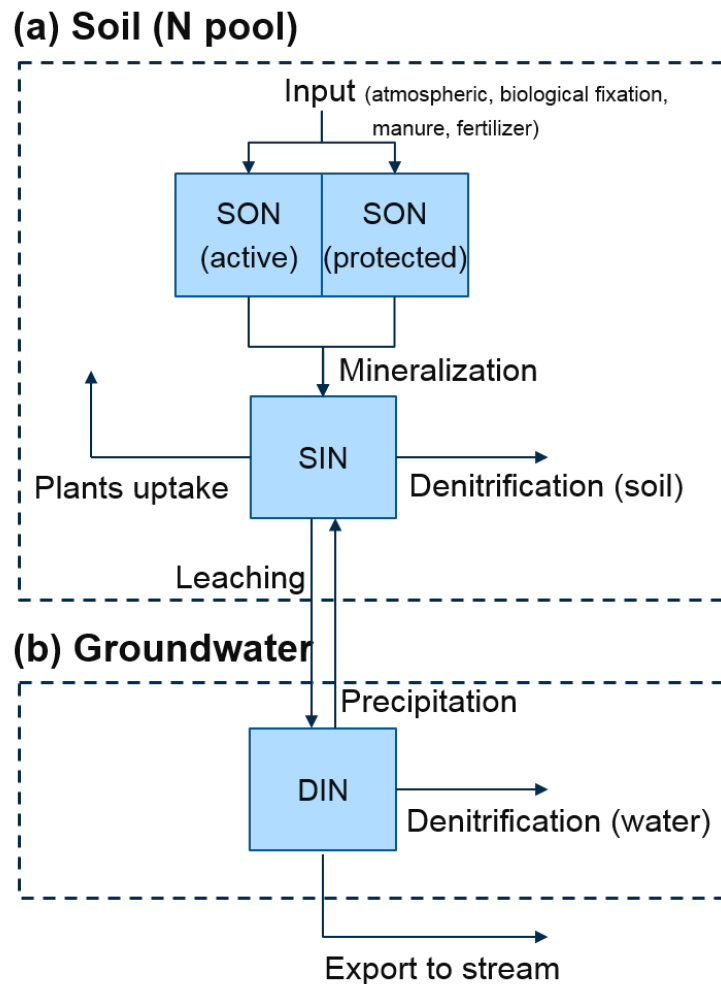
Parameter	Description	Range	Reference	Best-fit value
<u>N pool</u>				
d	Soil depth	Fixed	<i>Yang et al.</i> [2018]	0.5 m
N_{Input}	N external input	Fixed	<i>Nguyen et al.</i> [2021]	180 kg ha ⁻¹ yr ⁻¹
h	protection coefficient	Fixed	<i>Van Meter et al.</i> [2017]	0.3 [-]
k_a	Mineralization coef. (DON _a)	[0 - 0.7]	<i>Yang et al.</i> [2021]	0.011 day ⁻¹
k_p	Mineralization coef. (DON _p)	[0 - 0.7]	<i>Yang et al.</i> [2021]	0.0008 day ⁻¹
λ_s	Denitrification coef. (soil)	[0 - 0.7]	<i>Yang et al.</i> [2021]	0.0007 day ⁻¹
$p1$	Parameter for plants-uptake	[60 - 160]	<i>Van Meter et al.</i> [2017]	160 kg ha ⁻¹
$p2$	Parameter for plants-uptake	[0 - 10]		9.8 kg ha ⁻¹
$p3$	Parameter for plants-uptake	[1 - 60]		25.6 day
$p4$	Parameter for plants-uptake	Fixed		63 day
a	Leaching factor	[0 – 100]		0.154 [-]
<u>Transport</u>				
λ	Denitrification coef. (water)	[0 - 0.7]	<i>Yang et al.</i> [2021]	0.0072 day ⁻¹
a_L	Longitudinal dispersity	Fixed		8 m
a_T	Transverse dispersivity	Fixed		0.8 m

274

275 The N pool is positioned on the top part of the aquifer, used as a boundary condition for the DIN (nitrate) transport.
 276 Advective-dispersive transport of DIN in the flow system is simulated using HydroGeoSphere (Figure 2b).
 277 Degradation (denitrification in groundwater) during transport is considered as a first order process. Degradation is not
 278 considered on the land surface (denitrification in surface flow), where aerobic conditions likely deactivate
 279 denitrification and residence time is short. To implement the evapoconcentration effect in the transport model, ET is
 280 assumed to remove DIN mass without altering the DIN concentration of the water, and to inject that mass back to the
 281 SIN pool. This represents a precipitation process from DIN to SIN, which is the inverse process of leaching (Figure
 282 2b). There are two reasons for doing that: (i) the physical process of ET causing the immobilization of DIN can be
 283 mathematically considered, and (ii) the N mass balance can be conserved as the plants-uptake is already considered
 284 in the N pool according to the plant growth function (Equation 4 and 5), being independent from the ET flux.

285 Regarding the parameters, the soil depth, within which the N pool is implemented, is set to 0.5 m. N external input is
 286 180 kg ha⁻¹ yr⁻¹ according to Nguyen et al. (2021), where the nitrate balance was simulated for the larger upper Selke
 287 catchment that contained our studied catchment. The external N input is assumed to be spatiotemporally constant due
 288 to the limited information on its variation in space and time. The protection coefficient h is fixed as 0.3 according to
 289 the values reported in *Van Meter et al.* [2017]. The sowing date $p4$ is fixed as 63 days according to the fact that sowing

290 activities and plant growth start in early March. Longitudinal and transverse dispersivity values were 8 m and 0.8 m,
 291 respectively. Other parameters were set to be adjustable and calibrated (Table 2).



292
 293 **Figure 2.** Conceptual framework for nitrogen (N) fluxes (a) in the soil (N pool), and (b) after leaching into the
 294 groundwater.

295

296

297 ***Transport calibration***

298 As the flow parameters (e.g., hydraulic conductivity and porosity) were already calibrated in *Yang et al.* [2018] using
 299 data sets of discharge and groundwater levels. In this study, the calibration was only performed for the transport to get
 300 reasonable parameter values for the N pool and N transport. The software package PEST [*Doherty and Hunt, 2010*]
 301 was used. PEST uses the Marquardt method [*Marquardt, 1963*] to minimize a target function by varying the values
 302 of a given set of parameters until the optimization criterion is reached. We used the measured C_D and N surplus as the
 303 target variables for comparison with the simulated ones. The N surplus, which is the annual amount of N remaining
 304 in the soil after consumption by plant-uptake, was estimated as $48.8 \text{ kg ha}^{-1} \text{ yr}^{-1}$ [*Yang et al., 2021*]. As two different

305 data sets (C_Q and N Surplus) were used, a weighting scheme was used such that the defined multi-objective function
306 was not dominated by one data set.

307 Note that the entire model calibration (for flow and transport) actually followed a procedure of two steps: first for
308 flow, and second for transport. Alternatively, the flow and transport parameters can be calibrated at one step by
309 defining the multi-objective function using all the data sets (discharge, groundwater levels, C_Q and N surplus). The
310 potential effect of the two different calibration procedures on the modeling results should be further explored, however,
311 being out of the main focus of this study. We consider the two-step calibration procedure to be acceptable, because
312 our result showed that it was sufficient to reach an acceptable model performance for both flow and transport
313 (described later).

314 Several transport parameters were fixed at the values selected according to prior information, such that the degree of
315 freedom in the calibration can be reduced as much as possible (Table 2). In total eight parameters were adjustable and
316 calibrated, because they were the key parameters to determine the N fluxes in soil and groundwater. Their adjustable
317 ranges were selected according to the literature or to cover the values that the parameters can realistically reach (Table
318 2). The calibration was carried out for the period from Jul 1999 to Jul 2003, during which the data sets are available.
319 First, the flow and transport were simulated in the catchment of the base scenario (original topography, section 2.1).
320 Secondly, PEST was used to obtain a best fit between the simulated results and the data sets by varying the parameter
321 values. Note that the simulation period from Jul 1999 to Jul 2003 was only used for model calibration, rather than for
322 the actual simulations with the eleven catchments of different topographic slope. After calibration, the model with the
323 best-fit parameter values can well replicate the measured C_Q with a Nash-Sutcliffe efficiency (NSE) of 0.75 (see Figure
324 S1 in the supporting information). The simulated N surplus was $50.7 \text{ kg ha}^{-1} \text{ yr}^{-1}$, comparable to the measured value.

325 The best-fit parameter values from the base scenario were used for all other scenarios with catchments of different
326 topographic slope, assuming that the parameters do not change with the change of topographic slope. In total, we
327 simulated the flow and nitrate transport for eleven scenarios (11 catchments of different topographic slope). For each
328 scenario, the simulations were run for 100 years with identical boundary conditions for each year. The first 99 years
329 were used as a spin-up phase to assure a dynamic equilibrium (i.e. to achieve simulated variables, such as heads and
330 concentrations, that are identical between years), and the last year was used for actual observation and analysis. The
331 CPU time of each simulation was ~ 4 hours.

332 **3.2 Water ages**

333 The water stored in a catchment (storage), Q and ET can all be characterized by age distributions, for they comprise
334 water parcels of different age from precipitation events that occurred in the past. The age distributions need to be
335 calculated for each aforementioned scenario to assess the responses of water ages on catchment topographic slope.
336 Our model setup (with virtual catchments and identical climate for each year) allowed us to perform long-term
337 numerical tracer experiments and to extract the age distributions.

338 We assumed that inert tracers of uniform concentration existed in precipitation. The tracers were applied to the land
339 surface as a third-type (Cauchy) boundary condition and were subjected to transport modeling. Tracer can exit the

340 aquifer via the outfluxes Q and ET. We considered a period of 200 years for the tracer experiments, which was
 341 sufficiently long to ensure convergence of the computed water ages. The 200 years period was partitioned into 2400
 342 months ($\Delta t = 1$ month). A different tracer was used for each of the periods resulting in a total of 2400 distinct tracers.
 343 The injection of tracer i started with the precipitation at the beginning of its associated period t_0^i and lasted throughout
 344 the period. The advective-dispersive multi-solute transport was simulated using HydroGeoSphere. The first 199 years
 345 of the simulation period were used as a spin-up phase to ensure a dynamic equilibrium of the calculated ages,
 346 minimizing the influence of the initial conditions. The last year was used for the actual observations and the
 347 computation of age distributions. Solving the transport of the 2400 tracers would be computationally expensive.
 348 However, because the climate (flow boundary conditions) was identical for each year, the transport simulation was
 349 performed only for the first 12 tracers that covered the course of a year. Based on these results, the results for the other
 350 2388 tracers were manually reproduced (e.g., by shifting the concentration breakthrough curves of the 12 tracers in
 351 time while maintaining the shapes).

352 For each tracer, the breakthrough curves of the mass-fluxes of Q and ET, as well as the mass in storage were reported.
 353 For a specific time t , the age distributions for Q/ET/storage were computed by calculating the mass fraction of each
 354 tracer using:

$$355 \quad p_{Q/ET/S}(T, t) = \frac{M^i(t)}{\Delta t \sum M^i(t)} \quad (9)$$

356 where $p_Q(T, t)$, $p_{ET}(T, t)$ are the age distributions of Q, ET (equivalent to backward transit time distributions - TTDs),
 357 and $p_S(T, t)$ is the age distributions of water in storage (equivalent to the residence time distribution - RTD). $M^i(t)$ is
 358 the mass-flux of the tracer i in Q or ET, or the mass stored in catchment at time t , $\sum M^i(t)$ is the sum of $M^i(t)$ over
 359 all tracers. T is the age ranging within $[t - t_0^i - \Delta t, t - t_0^i]$ for tracer i .
 360

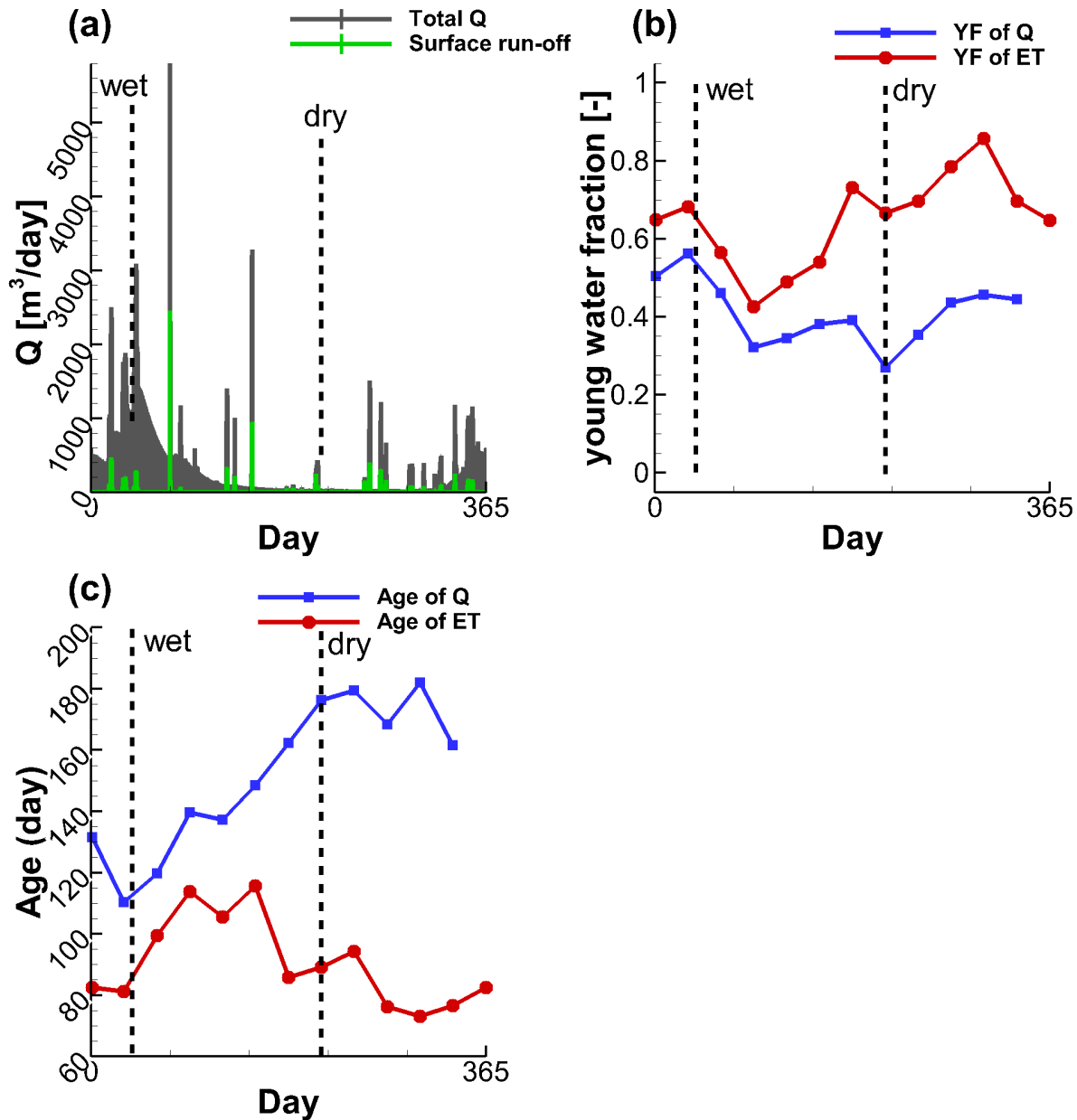
361 For each scenario, the CPU time of the tracer experiment was ~8 hours. Based on the age distributions, we calculated
 362 the mean discharge age $T_Q(t)$, which is equivalent to the mean discharge transit time (simply referred to as ‘discharge
 363 age’ in the following sections). We calculated the young water fraction in streamflow $YF_Q(t)$, which is the fraction of
 364 streamflow with an age younger than three months (also referred to as ‘young streamflow fraction’ [Jasechko *et al.*
 365 2016]). Similarly, the ET age $T_{ET}(t)$ and the young water fraction in ET $YF_{ET}(t)$ can be calculated as well (more
 366 details are described in Text S1 of the supporting information). Their responses to changes in topographic slope were
 367 analyzed.
 368

369 **4 Results and discussion**

370 **4.1 Dynamics of water ages and nitrogen fluxes**

371 Driven by the seasonality of the climate, the simulated Q, the young water fractions YF , and the water ages all show
 372 seasonal fluctuations. Figure 3 shows these fluctuations for the base scenario (original topography). Q reaches its
 373 maximum towards the end of the wet winter in late February and reaches its minimum during the drier late summer

374 in mid-September. Total Q consists of a portion of groundwater discharge (including the flow via vadose zone) and a
 375 portion generated via surface-runoff during events of high precipitation (Figure 3a). The calculated YF_{ET} is smallest
 376 in April and largest in November (Figure 3b), while YF_Q is smallest in August and largest in February. ET generally
 377 has larger young water fractions than Q as ET has a higher probability to remove young water from the shallow soil
 378 rather than the older water from the deeper aquifer. Especially during the dry season (summer), most precipitation can
 379 be quickly removed by ET. The water ages of Q and ET show generally opposite fluctuation patterns for YF (Figure
 380 3c). The ET age ranges from 70 to 115 days, being younger than Q that has the age ranging from 109 to 180 days.



381
 382 **Figure 3.** Simulated (a) Q, (b) young water fractions in streamflow (YF_Q) and evapotranspiration (YF_{ET}), and (c) water
 383 ages for the catchment of the base scenario. The YF and water ages are monthly averages.

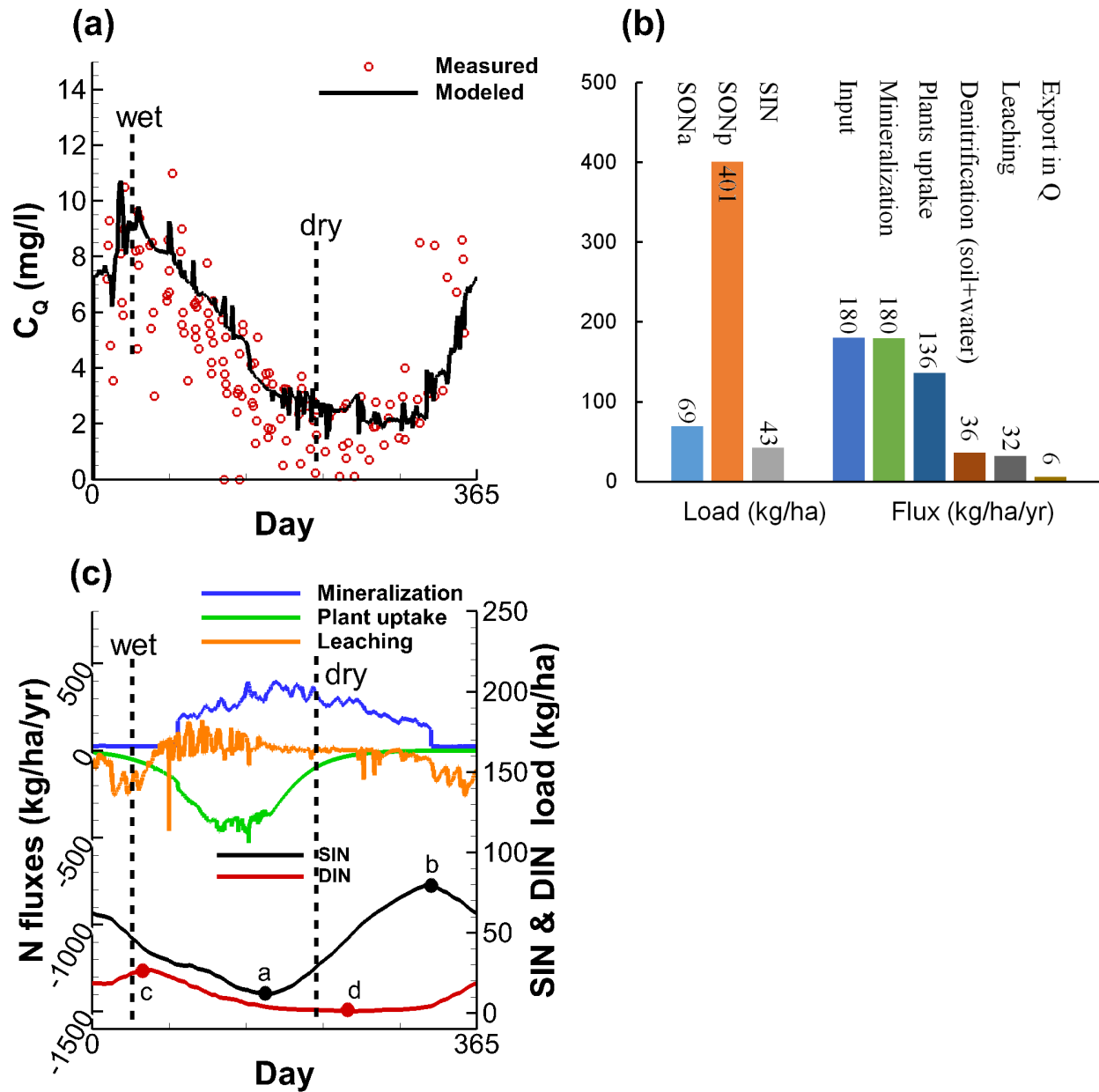
385 The simulated C_Q shows strong seasonality with maxima in the wet and minima in the dry period, fitting the measured
386 C_Q data well (Figure 4a). Figure 4b lists the calculated annual N mass balance in the catchment of the base scenario.
387 The organic (SONa + SONp) and inorganic (SIN) N load in the soil are 470 kg ha^{-1} and 43 kg ha^{-1} , respectively. The
388 SON accounts for 92% of the total N load, which is consistent with the study of Stevenson [1995] where the organic
389 N fraction was reported to be greater than 90%. The mineralization converts SON into SIN with a rate of 180 kg ha^{-1}
390 yr^{-1} . This rate is equal to the external N input because this way a steady-state of the annual N mass balance was reached
391 in the simulations. About 76% of the input N flux is taken up by the vegetation ($136 \text{ kg ha}^{-1} \text{ yr}^{-1}$). 20% is consumed
392 by denitrification ($36 \text{ kg ha}^{-1} \text{ yr}^{-1}$), either in the soil (before leaching) or in the groundwater (after leaching). The
393 remaining 4% reaches the stream water and is exported out of the catchment ($6 \text{ kg ha}^{-1} \text{ yr}^{-1}$). The simulated
394 mineralization flux is within the range of $[14\text{--}187] \text{ kg ha}^{-1} \text{ yr}^{-1}$ reported by *Heumann et al.* [2011] for their study sites
395 in central Germany. The simulated plant uptake and leaching fluxes are comparable to the values suggested in Nguyen
396 et al. [2021] for the same area ($120 \text{ kg ha}^{-1} \text{ yr}^{-1}$ for plant uptake and $[15\text{--}60] \text{ kg ha}^{-1} \text{ yr}^{-1}$ for leaching). The simulated
397 denitrification rate is within the range $[8\text{--}51] \text{ kg ha}^{-1} \text{ yr}^{-1}$ reported in Hofstra and Bouwman [2005] for 336 agricultural
398 soils located worldwide. Moreover, 80% and 20% of the leaching N are consumed by denitrification during transport
399 in the groundwater and exported to stream water, respectively. These portions are generally comparable to those
400 reported in Nguyen et al. [2021] (61% and 39%, respectively). Therefore, the simulated N loads and fluxes for the
401 catchment of the base scenario are considered to be acceptable.

402 Figure 4c shows the temporal variation of the N load and fluxes. It demonstrates that low levels of SIN are maintained
403 by high plant-uptake before the dry summer arrives (May – June), such that there is little SIN available for leaching.
404 The SIN load reaches its minimum when plant uptake reaches its maximum (marker a in Figure 4c). The cessation of
405 plant-uptake during the dry period leads to the increase of the SIN load as well as the increase of the leaching rate.
406 The mineralization in winter is significantly reduced due to the dropping temperatures, cutting the SIN supply. This
407 results in the SIN load reaching its high peak in the middle of November (marker b in Figure 4c) and subsequent
408 decrease due to increased leaching and eventually plant uptake. These seasonal fluctuation patterns are generally
409 consistent with the knowledge of N fluxes reported in previous studies [Dupas et al., 2017; Nguyen et al., 2021]. For
410 DIN load in water, it reaches its maximum generally when the leaching weakens in the beginning of March (marker c
411 in Figure 4c), and reaches the minimum just before the leaching process becomes active again in the end of August
412 (marker d in Figure 4c). These low and high peaks of SIN and DIN loads can also be identified by their spatial
413 distributions in the catchment (see Figure S2 in the supporting information).

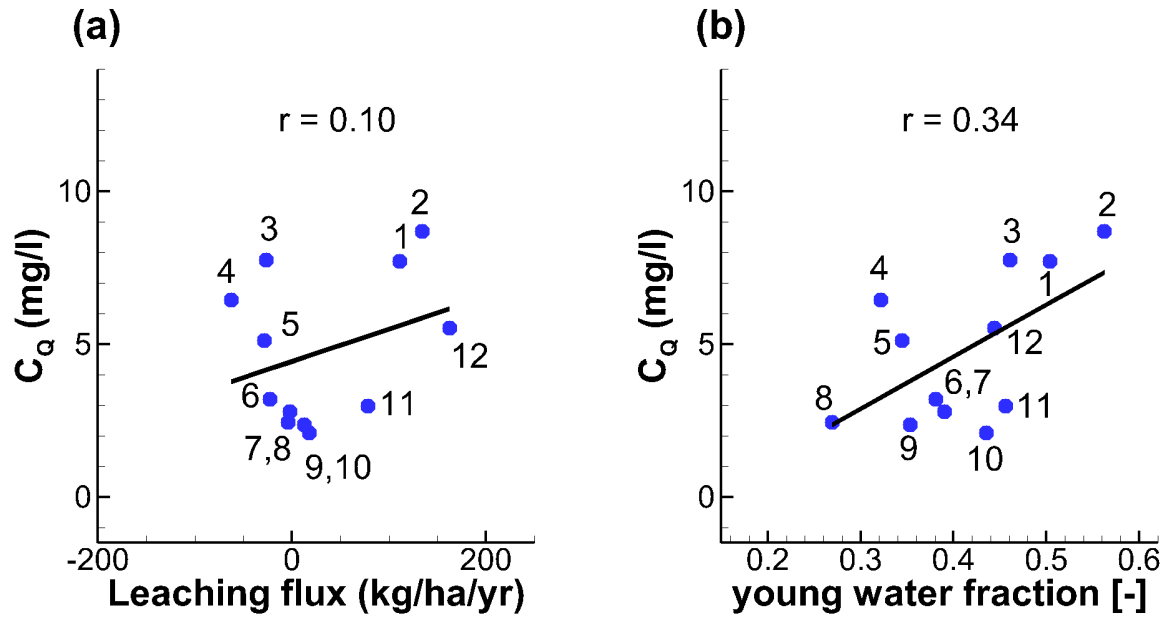
414 Seasonal variations of C_Q can be directly influenced either by the fluctuation of the nitrate leaching into groundwater,
415 or by fluctuations in the degradation in groundwater associated with varying transit times (quantified by the young
416 water fraction in streamflow YF_Q). These two influences represent the effect from the variability in N source and in N
417 transport, respectively. Linear regression analysis shows that C_Q is correlated with leaching flux rate and YF_Q with
418 Spearman rank-correlation coefficients of 0.1 and 0.34, respectively (Figure 5). The seasonal fluctuations of C_Q and
419 leaching flux are temporally out of phase. The maximum leaching occurs in December, while the maximum C_Q is

420 reached two months later in February (Figure 5a). The minimum leaching occurs in April, while the minimum C_Q is
421 reached around September. This behavior indicates that C_Q responds later to the changes in N leaching, which is
422 reasonable because the leaching nitrate needs time to travel from the shallow soil to streamflow. The fluctuation of
423 C_Q and YF_Q are more synchronized, proven by the fact that both maxima are reached in February (wet, Figure 5b) and
424 minima occur generally in the dry summer time. Field observations in mountainous central German catchments also
425 indicate that C_Q varies seasonally, with maxima during the wet winter and minima during the dry summer [Dupas et
426 al., 2017]. These seasonal fluctuations of C_Q and YF_Q were frequently explained using the “inverse storage effect”
427 [Harman, 2015; Yang et al. 2018]: during the wet season Q has a strong preference for young water associated with
428 higher concentrations, which would not occur during dry periods due to the deactivation of the shallow fast flow
429 processes. These patterns generally suggest that the C_Q fluctuation is more attributed to the variability in the N
430 transport rather than to the variability in the N source, echoing previous observations that 80% of the leaching N mass
431 is degraded during transport. However, it is still hard to tell whether the N source or the N transport is dominating the
432 C_Q fluctuation.

433



435
 436 **Figure 4.** Simulated (a) In-stream nitrate concentration C_Q , (b) N loads and fluxes, and (c) time-variable N fluxes for
 437 the catchment of the base scenario. Note that the measured C_Q in (a) includes all the measurements from 2001 to 2010.
 438

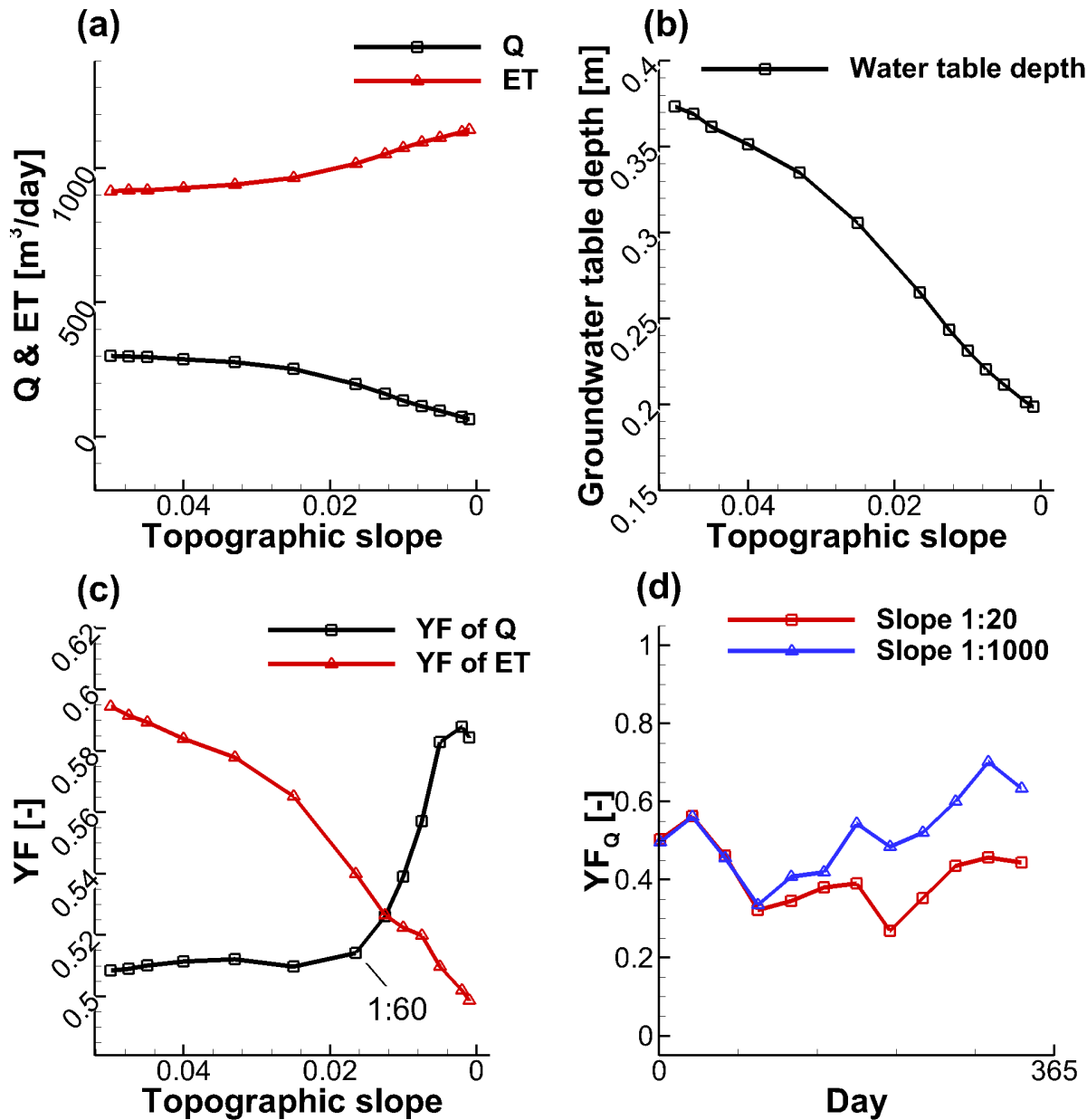


439
 440 **Figure 5.** Comparing the monthly averaged C_Q with (a) the leaching flux and (b) the young water fractions of Q. The
 441 black lines are linear fits of the two variables, with r being the Spearman rank-correlation coefficient. The numbers
 442 refer to the months.

443

444 4.2 Effect of topographic slope on flow

445 With the help of our simulations, it is possible to systematically explore the influence of topographic slope on the
 446 water flow and N fluxes. Figure 6 shows the responses of temporally-averaged Q and ET, the groundwater table depth,
 447 and flow weighted mean YF_Q and YF_{ET} to the changes of topographic slope. Under a constant climate, the changes of
 448 topographic slope can reshape the water flow via influencing flow partitioning between Q and ET. More water is taken
 449 up by ET and less water becomes Q in flatter landscapes (Figure 6a). These patterns can be explained by the change
 450 of groundwater table depth (Figure 6b), as shallower groundwater tables can be reached by the vegetation in flatter
 451 landscapes where ET therefore has a higher chance to remove water from the subsurface. The simulated YF_Q and YF_{ET}
 452 show generally increasing and decreasing patterns, respectively, when the topographic slope decreases (Figure 6c),
 453 demonstrating that young streamflow is more prevalent in flatter landscape and young ET is more prevalent in steeper
 454 landscapes. However, the increasing pattern of YF_Q does not continue in steep catchments with slopes $> 1:60$.
 455 Topographic slope changes YF_Q not only in terms of its mean value, but also in terms of its temporal variation. Figure
 456 6d indicates that the maximum and minimum YF_Q are reached in February and August for the steepest catchment
 457 (slope 1:20), respectively, and in November and April for the flattest catchment (slope 1:1000).



459

460 **Figure 6.** The simulated (a) Q and ET, (b) spatially-averaged depth of the groundwater table from the land surface,
 461 (c) young water fraction in streamflow YF_Q and evapotranspiration YF_{ET} , in relation to the topographic slope for the
 462 simulated catchments. (d) temporal variations of YF_Q for a steep landscape (slope 1:20) and a flat land scape (slope
 463 1:1000).

464

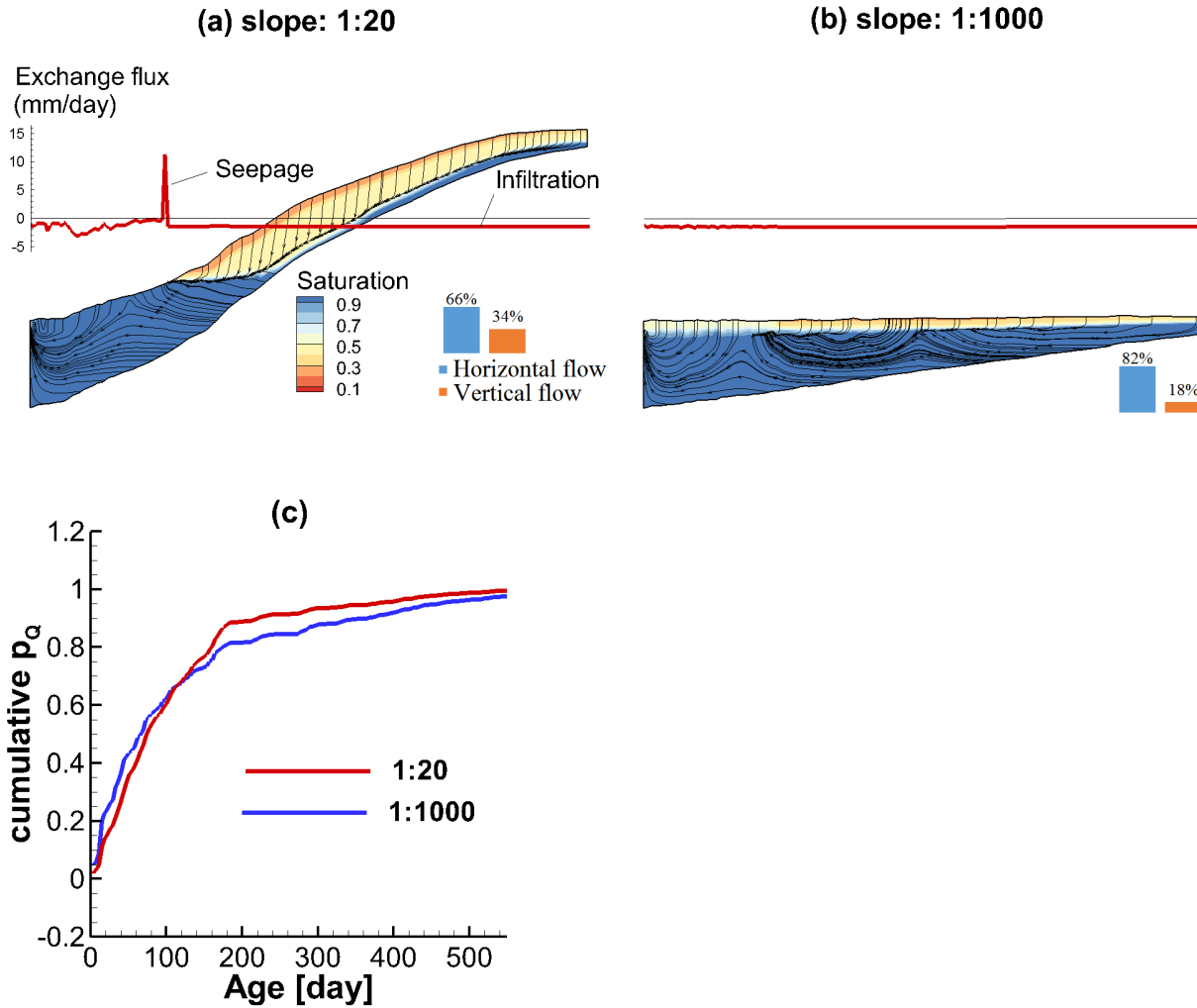
465 Interpreting the response of the YF_Q to topographic slope mechanistically requires a closer look at the flow processes
 466 using a cross-sectional view. We plotted the subsurface flow fields for the wet season at a cross-section of the
 467 catchments with slopes 1:20 and 1:1000 (Figure 7).

468 Figure 7a reveals that the hillslope part of the catchment with a slope of 1:20 is largely unsaturated so that the flow
469 paths in this area are characterized by vertical infiltration. In contrast, the valley bottom is fully saturated. Overall,
470 34% of the subsurface domain is characterized by vertical flow (flow in 34% of the total aquifer volume is more
471 vertical than horizontal). For this scenario two main discharge routes to the stream can be identified: (i) A fraction of
472 the groundwater flows through the fully saturated zone and exits the aquifer to the stream, and (ii) another fraction
473 exits the aquifer via seepage near to where the groundwater table intersects the land surface, indicated by a large
474 exchange flux (from subsurface to surface, positive). The seepage represents a preferential flow path allowing for
475 discharge via overland flow instead of discharge via the sub-surface with longer transit times. Note that both of the
476 discharge routes provide the pathways for the rainfall falling on the top hillslope to reach the stream.

477 When the slope is reduced to 1:1000, the flow pattern experiences significant changes (Figure 7b) compared to the
478 catchment with a slope of 1:20. Several hydrologic studies have described two different flow systems in aquifers: (i)
479 a recharge-limited system where the thickness of the unsaturated zone is sufficient to accommodate any water-table
480 rise and thus the elevation of the groundwater table is limited by the recharge, and (ii) a topography-limited system
481 where the groundwater table is close or connected to the land surface such that any fluctuation in groundwater table
482 can result in considerable change in surface runoff [Werner and Simmons, 2009; Michael et al., 2013]. In the selected
483 cross sections, the steeper one (slope 1:20) is a partially topography-limited system (Figure 7a) (the hillslope is
484 recharge-limited while the valley bottom is topography-limited). The flat one (slope 1:1000) is transformed into a
485 fully recharge-limited system (from Figure 7b) due to the reduced hydraulic head gradients. This transformation leads
486 to three main effects: (i) The seepage flow vanishes because the groundwater table disconnects from the land surface.
487 The seepage route that would discharge water from the top of hillslope to the stream is cut off, (ii) the infiltration
488 processes is weakened, indicated by the fact that the portion of subsurface domain characterized by vertical flow is
489 reduced from 34% to 18%, and (iii) local flow cells are more likely to form, where water infiltrates to the aquifer and
490 eventually exits the aquifer via ET rather than via flow to the stream (Figure 7b, the local flow cells are more
491 pronounced in the dry season, see Figure S3-b in the supporting information).

492 Because of the three aforementioned effects, the connectivity between the stream and the more distant hillslopes is
493 significantly reduced. Precipitation falling farther from the stream has a lower chance to reach the stream and a higher
494 change to be intercepted by ET on its way to the stream. The hillslope that used to generate old streamflow does not
495 contribute to streamflow anymore. While precipitation water close to the stream has a higher chance to contribute to
496 streamflow. We concluded that the increase of the YF_Q in flat landscapes is due to this reduction of the longer flow
497 paths and the persistence of shorter flow paths, as indicated by the computed TTDs (Figure 7c).

498



499 **Figure 7.** Cross-sectional view of saturation, flow paths, and exchange fluxes between the surface and the subsurface
500 in the wet season (February) for catchments with topographic slope (a) 1:20, and (b) 1:1000. The cross-section is
501 marked in Figure 1a. The black lines represent the flow paths. The red curves show exchange fluxes (along the cross-
502 sectional profiles), positive values indicate seepage to the land surface and negative values indicate infiltration to the
503 subsurface. (c) The computed cumulative TTDs for Q during the wet season (February), for the catchment with
504 topographic slope of 1:20 and 1:1000.
505

506
507 In summary, we identified a generally increasing pattern of YF_Q in response to the decreasing topographic slope. When
508 the landscape becomes flatter, the hydraulic head gradient as the main driving force changes the aquifer from a
509 partially topography-limited system to a recharge-limited system that is more likely to form local flow cells.

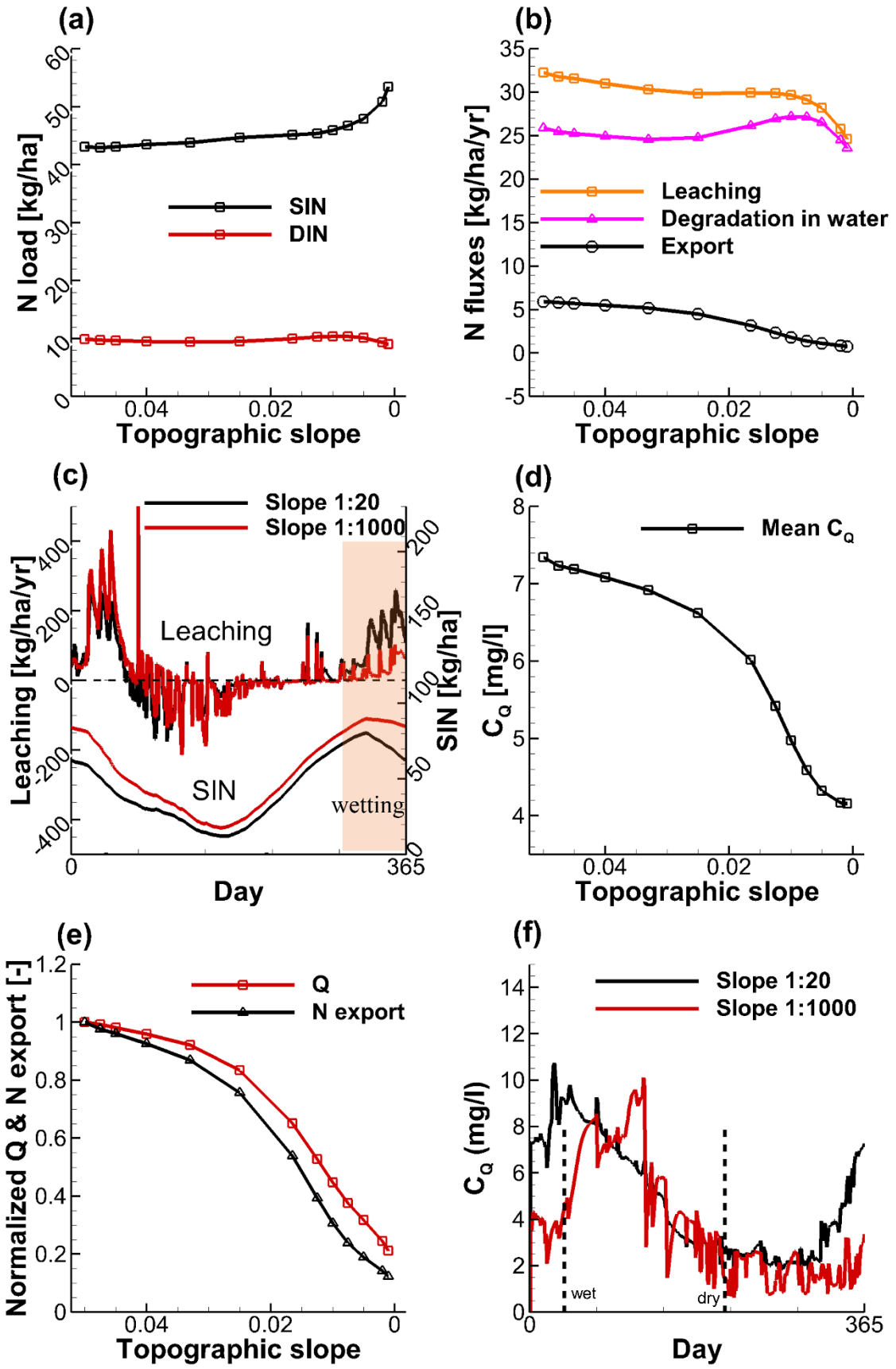
510
511 **4.3 Effect of topographic slope on N export**

512 Simulated results show that the topographic slope can influence the N loads and fluxes in catchments. Figure 8a
513 demonstrates that SIN tends to be higher in flatter and lower in steeper landscapes. This generally indicates that a flat

514 landscape has a higher potential to retain N in the soil. However, the DIN is not significantly influenced by the
515 topographic slope. N fluxes of leaching and export to the stream exhibit the opposite pattern. For the N fluxes, the
516 leaching into groundwater decreases with the decrease of topographic slope (Figure 8b). This is mainly because the
517 flow velocity (influencing the leaching rate according to equation 6) in flatter landscape is lower due to the reduced
518 hydraulic head gradient. Comparing the time-variable leaching between the steepest and flattest catchments (slope
519 1:20 and 1:1000, Figure 8c), it can be observed that the leaching reduction in the flatter landscape mainly occurs in
520 the wetting period (Nov to Dec). This may be because the response of flow velocity in the flatter catchment is not as
521 large as that in the steeper catchment when the system transitions from dry to wet conditions. A large portion of the
522 leached N mass has been degraded during transport in the groundwater, with the fraction rising from 80% in the
523 steepest landscape to 95% in the flattest landscape (Figure 8b). Mechanically, the reduced connectivity between the
524 stream and more distant hillslopes in flatter landscapes inhibits the N export to the stream promoting the degradation
525 by increasing the N residence time in the catchment. Subsequently, the N export shows a decreasing pattern with the
526 decrease of topographic slope (Figure 8b).

527 The calculated flow-weighted mean C_Q shows a decreasing trend in response to the decreasing topographic slope
528 (Figure 8d), from 7.3 mg l⁻¹ in the steepest catchment to 4.2 mg l⁻¹ in the flattest catchment. Even though both Q and
529 N export show decreasing patterns with the decrease of topographic slope, the N export decreases to a higher degree
530 than Q, indicated by the normalized values (Figure 8e). Comparing the time-variable C_Q between the steepest and
531 flattest catchments (slope 1:20 and 1:1000, Figure 8f), it can be observed that the topographic slope influences the C_Q
532 in two ways: (i) The C_Q is generally lower (but not always) in the flatter landscape over most of the time in a year, and
533 (ii) the high peaks of C_Q in flatter landscapes are delayed in time. However, the high concentrations always occur in
534 the wet periods (Jan – Apr) and low concentrations always occur in the dry periods (Jul – Oct).

535



537 **Figure 8.** The simulated (a) N loads, (b) N fluxes in relation to the topographic slope for the simulated catchments.
538 (c) Comparison of the time variable N loads and fluxes between a steep (slope 1:20) and a flat land scape (slope
539 1:1000). The simulated (d) flow-weighted mean C_Q , and (e) the normalized Q and N export (normalized to their values
540 of the base scenario) in relation to the topographic slope. (f) Comparison of the time variable C_Q between a steep
541 (slope 1:20) and a flat land scape (slope 1:1000). Note that for the leaching fluxes in (c), positive values are referred
542 to as the N leaching from the soil to the groundwater, negative values are referred to as the precipitation of N from
543 groundwater to the soil by the evapoconcentration effect. The vertical dashed lines indicate the time when the
544 catchment reaches the wettest (left) and the driest (right) conditions.

545

546 **4.4 Discussion**

547 *Jasechko et al.*, [2016] reported that (the logarithm of) catchment topographic slope was significantly negatively
548 correlated with young streamflow fractions with a spearman rank correlation of -0.36. This conclusion was made
549 statistically based on their observed 254 sites. Our numerical study based on the eleven catchments with different
550 slopes but identical climate conditions resulted in more physically-based information that goes beyond such statistical
551 correlations. Our results confirm that young streamflow fraction and slope generally exhibit a negative correlation.
552 Additionally, our results show that the young water fraction in ET is positively correlated with the slope.

553 From the steepest landscape to the flattest landscape, catchments are likely to transition from a partially topography-
554 limited flow system to a recharged limited system, due to the reduction of hydraulic gradient. The groundwater table
555 is closer to the land surface when the landscape becomes flatter. The larger young streamflow fraction in flatter
556 landscapes is consistent with the statement made by *Jasechko et al.* [2016] that the young streamflow fraction is more
557 prevalent in flatter catchments which are characterized by more shallow lateral flow and less vertical infiltration. This
558 phenomenon is also consistent with a negative correlation between groundwater table depth and young streamflow
559 fraction, which has been frequently reported [*Bishop et al.*, 2004; *Seibert et al.*, 2009; *Frei et al.*, 2010; *Jasechko et*
560 *al.*, 2016]. Using the insight into the flow processes of the catchment, we found that the connectivity between the
561 stream and the more distant hillslopes is reduced in flatter landscape, due to the reduced seepage flow, the weakened
562 infiltration and the formation of local flow cells that do not deliver flow to the stream. Our study points out that the
563 reduction of this connectivity, which results in the reduction of the longer flow paths and the persistence of shorter
564 flow paths, causes the increase of the young streamflow fraction.

565 Basically, the position of the groundwater table, flow path lengths and flow velocities, which are all different for
566 different topographic slopes, jointly affect the young streamflow fractions. Besides that, temporal variability of these
567 three factors drives the distinct responses of the young streamflow fraction to topographic slope between seasons. In
568 our simulated catchments, the negative correlation between young streamflow fraction and topographic slope is more
569 pronounced in the flat landscapes with slopes $< 1:60$. This demonstrates that the system is complex and apparently
570 contains various threshold effects disturbing a straightforward monotonous relationship between catchment
571 characteristics (e.g. slope) and young water fraction (or streamflow concentration). In this sense, systematically

572 investigating the reaction of the flow dynamics to catchment characteristic is necessary, rather than assuming a
573 straightforward cause-effect relationship that can be misleading.

574 Our results demonstrate that stream water quality is potentially less vulnerable in flatter landscapes. The flatter
575 landscapes tend to retain more N mass in the soil and export less N mass to the stream. This behavior can be attributed
576 to (i) the reduced leaching in flat landscapes since the decreased flow velocity physically reduces the potential of water
577 to solve and transport the solute, and (ii) the increased potential of degradation because the connectivity between the
578 stream and hillslope is blocked (i.e. there is more time for decay). Our results also show that higher C_Q is more
579 prevalent in steeper landscapes. Note that this is concluded for average concentrations. Observations from the Selke
580 catchment, central Germany show that the C_Q is not always lower in flatter regions [Dupas *et al.*, 2017; Nguyen *et al.*,
581 2022]. In the future more attention should be paid to the temporal variation and the time-scale concerning the effect
582 of topographic slope on C_Q . Additionally, our results show that we can expect lower C_Q and higher young streamflow
583 fractions in flatter landscapes. This suggests that, with regard to the N transport in catchments, a large young
584 streamflow fraction is not sufficient for high levels of C_Q . This phenomenon has not yet been reported to the best of
585 our knowledge.

586 Concerning the seasonal variations of C_Q , our results showed that significant seasonal variation can be expected under
587 temperate humid climates regardless of topographic slope. The high peak concentrations occurred in the wet and the
588 low in the dry seasons, being consistent with the findings of previous studies [Benettin *et al.* 2015; Harman, 2015;
589 Kim *et al.*, 2016; Yang *et al.*, 2018]. However, the topographic slope can slightly shift the high peak concentrations in
590 time.

591

592 **4.5 Limitations and outlook**

593 The cross-comparison between catchments with differing topographic slopes provides physically-based insights into
594 the effects of topographic slope on nitrate export responses in terms of N fluxes and mean concentrations. However,
595 this study is limited in scope in that it neglects other factors that may also have important impacts on the young
596 streamflow and nitrate export processes:

597 First, our study only considered the aquifers that is unconfined with an impermeable base and prescribed heterogeneity.
598 Other catchment characteristics such as landscape aspect, catchment area, aquifer permeability or drainage ability,
599 aquifer depth, stream bed elevation, fractured bedrock permeability, bedrock slope and shape of basin can potentially
600 change the flow patterns and age composition in streamflow [McGlynn *et al.*, 2003; Broxton *et al.*, 2009; Sayama and
601 McDonnell, 2009; Stewart *et al.*, 2010; Jasechko *et al.*, 2016; Heidbüchel *et al.*, 2013, 2020; Zarlenga and Fiori,
602 2020]. For example, aquifers with high permeability or highly fractured bed rock are more likely to use deep rather
603 than shallow flow paths and preferential discharge routes that lead to rapid drainage. Apart from that, it was reported
604 that hydrological features such as precipitation variability, ET, antecedent soil moisture are also significantly linked
605 to transit times [Sprenger *et al.*, 2016; Wilusz *et al.* 2017; Evaristo *et al.*, 2019; Heidbüchel *et al.*, 2013, 2020]. For
606 example, compared to uniform precipitation, event-scale precipitation is more likely to trigger rapid surface runoff

607 and intermediate flow, such that the contribution of young water from storage to streamflow can be increased.
608 Therefore, further research should consider a more complex model structure involving various heterogeneity and
609 climate types.

610 Second, several main simplifications were used in the formulation of the nitrate transport processes. (i) Transport
611 modelling employed a constant degradation rate coefficient assuming that transit time was the only factor to determine
612 degradation. This assumption neglected other factors that can spatially and temporally affect denitrification rates, such
613 as temperature, redox boundaries (e.g., high oxygen concentration in shallow flow paths), the amount of other nutrients
614 (e.g. carbon), which also contribute to the seasonality in nitrate concentrations [Böhlke *et al.*, 2007]. Apart from that,
615 we did not account for the long-term (decades [Van Meter *et al.*, 2017]) nitrate legacy effect as the dissolved nitrate
616 in groundwater reservoirs degraded continuously in our model, which would not occur in older reservoirs where the
617 denitrification is very slow or deactivated (e.g. due to the lack of a carbon source). (ii) The N external input source
618 was uniformly applied across the land surface in our modelling. However, strong source heterogeneity may exist in
619 catchments. For example, the N external input varies between land uses or along the soil profile [Zhi *et al.*, 2019].
620 This spatial source heterogeneity could affect the seasonal variations of C_Q [Musolff *et al.*, 2017; Zhi *et al.*, 2019] and
621 should be considered in further research.

622 While the numerical model provided general insights, there was potential uncertainty in the simulated results. Firstly,
623 the aforementioned simplifications may introduce model structural errors. Secondly, the model calibration was only
624 constrained by limited data sets, which may lead to the non-uniqueness in the model parameters. Both of the aspects
625 may introduce uncertainty in the simulated N loads and fluxes. Future work should be devoted to better constrain the
626 model parameters, either by enhancing the concentration data quality through more frequent measurements or by
627 providing additional data sets related to the N pool. Despite these limitations, the numerical experiments in this study
628 could clearly identify the response of young streamflow and nitrate export to topographic slope under a humid seasonal
629 climate, and show that hydraulic gradient is an important factor causing flow field differences between the catchments.
630 This was achieved by using the advantages of a physically-based flow simulation that allows for a more mechanistic
631 evaluation of flow processes, which would be impossible with a purely data driven analysis based on, e.g., isotopic
632 tracers only.

633

634 **5 Conclusions**

635 Previous data driven studies suggested that catchment topographic slope impacts the age composition of streamflow
636 and consequently the in-stream concentrations of certain solutes [Jasechko *et al.*, 2016]. We attempted to find more
637 mechanistic explanations for these effects. We chose the small agricultural catchment ‘Schäferfetal’ in Central Germany
638 and, based on it, generated eleven synthetic catchments of varying topographic slope. The groundwater and overland
639 flow, and the N transport in these catchments were simulated using a coupled surface-subsurface model. Water age
640 compositions for Q and ET were determined using numerical tracer experiments. Based on the calculated flow patterns,
641 young water fractions in streamflow YF_Q , N mass fluxes and in-stream nitrate concentration C_Q , we systematically

642 assessed the effects of varying catchment topographic slopes on the nitrate export dynamics in terms of the mass fluxes
643 and annual mean concentration levels. The main conclusions of this study are:

- 644 • Under the considered humid climate, YF_Q is generally negatively correlated to topographic slope. When the
645 landscape becomes flatter, the hydraulic head gradient is the main driving force to change the aquifer from a
646 partially topography-limited system to a recharge-limited system, reducing the connectivity between the
647 stream and the more distant hillslopes. This change results in the reduction of longer flow paths and the
648 persistence of shorter flow paths, subsequently causing the flatter landscapes to generate younger streamflow.
- 649 • The flatter landscapes tend to retain more N mass in soil and export less N mass to the stream. These patterns
650 are attributed to (i) the reduced leaching in flat landscape as the decreased flow velocity physically reduces
651 the potential of water to transport the solute towards the stream, and (ii) the increased potential of degradation
652 as the connectivity between the stream and hillslope is blocked and the solute stays inside the aquifer longer.
- 653 • For the considered catchment, the annual mean C_Q shows a decreasing trend in response to the decreasing
654 topographic slope, because the N export decreases to a higher degree than Q. Flatter landscapes tend to
655 generate larger young streamflow fractions (but lower C_Q), suggesting that a large young streamflow fraction
656 is not sufficient for a high level of C_Q .

657 Overall, this study provided a mechanistic perspective on how catchment topographic slope affects young streamflow
658 fraction and nitrate export patterns. The use of a fully-coupled flow and transport model extended the approach to
659 investigate the effects of catchment characteristics beyond the frequently used tracer data-driven analysis. It can be
660 used for similar studies of other catchment characteristics and for other solutes. The results of this study improved the
661 understanding of the effects of certain catchment characteristics on nitrate export dynamics with potential implications
662 for the management of stream water quality and agricultural activity, in particular for catchments in temperate humid
663 climate with pronounced seasonality. Given the limitations of this study, future work should be devoted to improve
664 the degradation formulation, to investigate further catchment characteristics, as well as to consider various climate
665 types.

666

667

668 **Notation**

669 t [T] time

670 T [T] age / transit time / residence time

671 J [LT^{-1}] precipitation

672 ET [LT^{-1}] evapotranspiration

673 Q [LT^{-1}] discharge / streamflow

674 ps [-] age distribution of storage

675 $p_{ET/Q}$ [-] age distribution for evapotranspiration / discharge, equivalent to TTD

676 C [ML^{-3}] concentration

677 C_Q [ML⁻³] in-stream solute (nitrate) concentration
678 T_Q [ML⁻³] age (transit time) of discharge
679 YF_Q [-] young water fraction in streamflow, or young streamflow fraction
680 YF_{ET} [-] young water fraction in ET
681 SON [M L⁻²] soil organic nitrogen
682 SIN [M L⁻²] soil inorganic nitrogen
683 DIN [M L⁻²] dissolved inorganic nitrogen in water

684
685
686

687 **Code/Data availability**

688 All data used in this study are listed in the supporting information and uploaded separately to HydroShare [Yang,
689 2022].
690

691 **Author contributions**

692 JY: conceptualization, methodology, software, formal analysis, visualization, writing - review & editing; QW:
693 modelling, analysis, writing; IH: writing - review & editing; CL: conceptualization, methodology, review & editing;
694 YX: methodology; AM: conceptualization; JF: conceptualization, review & editing.
695

696 **Competing interests**

697 The authors declare that they have no conflict of interest.
698

699 **Acknowledgments**

700 This research was supported by the National Key Research and Development Project (JY & CL: 2021YFC3200500),
701 the National Natural Science Foundation of China (JY: 52009032, CL: 51879088), the Fundamental Research Funds
702 for the Central Universities (JY: B210202019), and the Natural Science Foundation of Jiangsu Province (CL:
703 BK20190023). We thank the editorial board for handling our manuscript, especially Prof. Dr. Insa Neuweiler and two
704 anonymous reviewers, whose constructive comments helped improve the manuscript.
705

706 **References**

707 Anis, M. R., & Rode, M. (2015). Effect of climate change on overland flow generation: A case study in central
708 Germany. *Hydrological Processes*, 29(11), 2478–2490.

709 Benettin, P., Y. van der Velde, S. E. A. T. M. van der Zee, A. Rinaldo, and G. Botter (2013), Chloride circulation in
710 a lowland catchment and the formulation of transport by travel time distributions, *Water Resources Research*, 49(8),
711 4619–4632, doi: 10.1002/wrcr.20309.

712 Benettin, P., J. W. Kirchner, A. Rinaldo, and G. Botter (2015), Modeling chloride transport using travel time
713 distributions at plynlimon, wales, *Water Resources Research*, 51(5), 3259–3276, doi:10.1002/2014WR016600.

714 Bishop, K., Seibert, J., Köhler, S. and Laudon, H. (2004), Resolving the Double Paradox of rapidly mobilized old
715 water with highly variable responses in runoff chemistry. *Hydrol. Process.*, 18: 185-189.
716 <https://doi.org/10.1002/hyp.5209>.

717 Botter, G., Bertuzzo, E., & Rinaldo, A. (2010). Transport in the hydrologic response: Travel time distributions, soil
718 moisture dynamics, & the old water paradox. *Water Resources Research*, 46(3).
719 <https://doi.org/10.1029/2009WR008371>.

720 Botter, G., Bertuzzo, E., & Rinaldo, A. (2011). Catchment residence and travel time distributions: The master equation.
721 *Geophysical Research Letters*, 38(11). <https://doi.org/10.1029/2011GL047666>.

722 Böhlke, J. K., M. E O'Connell, and K. L Prestegard (2007), Ground water stratification and delivery of nitrate to an
723 incised stream under varying flow conditions, *Journal of environmental quality*, 36, 664–80,
724 doi:10.2134/jeq2006.0084.

725 Broxton, P. D., P. A. Troch, and S. W. Lyon (2009), On the role of aspect to quantify water transit times in small
726 mountainous catchments, *Water Resour. Res.*, 45, W08427, doi:10.1029/2008WR007438.

727 Doherty, J., Hunt, R., 2010. Approaches to highly parameterized inversion – a guide to using PEST for groundwater-
728 model calibration. Technical Report, USGS Survey Scientific Investigations Report. 2010-5169.

729 Dupas, R., A. Musolff, J. W. Jawitz, P. S. C. Rao, C. G. Jäger, J. H. Fleckenstein, M. Rode, and D. Borchardt (2017),
730 Carbon and nutrient export regimes from headwater catchments to downstream reaches, *Biogeosciences*, 14(18),
731 4391–4407, doi:10.5194/bg-14-4391-2017.

732 Evaristo, J., Kim, M., van Haren, J., Pangle, L. A., Harman, C. J., Troch, P. A., & McDonnell, J. J. (2019).
733 Characterizing the fluxes and age distribution of soil water, plant water, and deep percolation in a model tropical
734 ecosystem. *Water Resources Research*, 55(4), 3307-3327.

735 Frei, S., Lischeid, G. and Fleckenstein J.H. (2010) Effects of micro-topography on surface-subsurface exchange and
736 runoff generation in a virtual riparian wetland – a modeling study, *Advances in Water Resources*, 33(11):1388-1401.

737 Haag, D., Kaupenjohann, M., 2001. Landscape fate of nitrate fluxes and emissions in central Europe: a critical review
738 of concepts, data, and models for transport and retention. *Agric. Ecosyst. Environ.* 86 (1), 1–21.

739 Harman, C. J. (2015), Time-variable transit time distributions and transport: Theory and application to storage-
740 dependent transport of chloride in a watershed, *Water Resources Research*, 51(1), 1–30, doi:10.1002/2014WR015707.

741 Harman, C. J. (2019). Age-Ranked Storage-Discharge Relations: A Unified Description of Spatially Lumped Flow
742 and Water Age in Hydrologic Systems. *Water Resources Research*, 55(8), 7143-7165.

743 Heidbüchel, I., P. A. Troch, and S. W. Lyon (2013). Separating physical and meteorological controls of variable transit
744 times in zero-order catchments. *Water Resources Research*, 49, 7644–7657, doi:10.1002/2012WR013149.

745 Heidbüchel, I., J. Yang, A. Musolff, P. Troch, T. Ferré, J. H. Fleckenstein (2020). On the shape of forward transit time
746 distributions in low-order catchments. *Hydrology and Earth System Sciences*, doi: 10.5194/hess-2019-440.

747 Hrachowitz, M., O. Fovet, L. Ruiz, and H. H. G. Savenije (2015), Transit time distributions, legacy contamination
748 and variability in biogeochemical 1/f scaling: how are hydrological response dynamics linked to water quality at the
749 catchment scale?, *Hydrological Processes*, 29(25), 5241–5256, doi:10.1002/hyp.10546.

750 Heumann, S., Ringe, H., Böttcher, J., 2011. Field-specific simulations of net N mineralization based on digitally
751 available soil and weather data. I. Temperature and soil water dependency of the rate coefficients. *Nutr. Cycl.*
752 *Agroecosyst.* 91 (2), 219–234. <https://doi.org/10.1007/s10705-011-9457-x>.

753 Hofstra, N., Bouwman, A.F., 2005. Denitrification in agricultural soils: summarizing published data and estimating
754 global annual rates. *Nutr. Cycl. Agroecosyst.* 72 (3), 267–278. <https://doi.org/10.1007/s10705-005-3109-y>.

755 Hrachowitz, M., P. Benettin, B. M. Van Breukelen, O. Fovet, N. J. Howden, L. Ruiz, Y. Van Der Velde, and A. J.
756 Wade (2016), Transit times-the link between hydrology and water quality at the catchment scale, *Wiley*
757 *Interdisciplinary Reviews: Water*, 3(5), 629–657.

758 Jasechko, S., Kirchner, J., Welker, J. et al. Substantial proportion of global streamflow less than three months old.
759 *Nature Geosci* 9, 126–129 (2016). <https://doi.org/10.1038/ngeo2636>

760 Kaandorp, V. P., Louw, P. G. B., Velde, Y., & Broers, H. P. (2018). Transient Groundwater Travel Time Distributions
761 and Age - Ranked Storage - Discharge Relationships of Three Lowland Catchments. *Water Resources Research*, 54,
762 4519– 4536. <https://doi.org/10.1029/2017WR022461>

763 Kim, M., L. A. Pangle, C. Cardoso, M. Lora, T. H. Volkmann, Y. Wang, C. J. Harman, and P. A. Troch (2016), Transit
764 time distributions and storage selection functions in a sloping soil lysimeter with time-varying flow paths: Direct
765 observation of internal and external transport variability, *Water Resources Research*, 52(9), 7105–7129.

766 Knoll, L., Breuer, L., & Bach, M. (2020). Nation-wide estimation of groundwater redox conditions and nitrate
767 concentrations through machine learning. *Environmental Research Letters*, 15, 064004. [https://doi.org/10.1088/1748-](https://doi.org/10.1088/1748-9326/ab7d5)
768 [9326/ab7d5](https://doi.org/10.1088/1748-9326/ab7d5).

769 Kolbe, T., de Dreuzy, J. R., Abbott, B. W., Aquilina, L., Babey, T., Green, C. T., et al. (2019). Stratification of
770 reactivity determines nitrate removal in groundwater. *Proceedings of the National Academy of Sciences*, 116(7),
771 2494–2499. <https://doi.org/10.1073/pnas.1816892116>.

772 Li, Y., Chen, Y., Li, Z., 2019. Dry/wet pattern changes in global dryland areas over the past six decades. *Glob. Planet.*
773 *Chang.* 178, 184–192. <https://doi.org/10.1016/j.gloplacha.2019.04.017>.

774 Lindström, G., C.P. Pers, R. Rosberg, J. Strömqvist, and B. Arheimer (2010): Development and test of the HYPE
775 (Hydrological Predictions for the Environment) model – A water quality model for different spatial scales, *Hydrol.*
776 *Res.*, 41.3–4, 295–319, 2010.

777 Marquardt, D.W., 1963. An algorithm for least-squares estimation of nonlinear parameters. *J. Soc. Ind. Appl. Math.*
778 11 (2), 431–441.

779 McGlynn, B., J. McDonnell, M. Stewart, and J. Seibert (2003), On the relationships between catchment scale and
780 streamwater mean residence time, *Hydrol. Processes*, 17, 175– 181, doi:10.1002/hyp.5085.

781 Michael, H.A., Russoniello, C.J., Byron, L.A., 2013. Global assessment of vulnerability to sea-level rise in
782 topography-limited and recharge-limited coastal groundwater systems. *Water Resour. Res.* 49, 1–13.

783 Musolff, A., C. Schmidt, B. Selle, and J. H. Fleckenstein (2015), Catchment controls on solute export, *Advances in*
784 *Water Resources*, 86, 133–146.

785 Musolff, A., J. H. Fleckenstein, P. S. C. Rao, and J. W. Jawitz (2017), Emergent archetype patterns of coupled
786 hydrologic and biogeochemical responses in catchments, *Geophysical Research Letters*, 44(9), 4143–4151,
787 doi:10.1002/2017GL072630.

788 Nguyen, T. V., Kumar, R., Lutz, S. R., Musolff, A., Yang, J., & Fleckenstein, J. H. (2021). Modeling nitrate export
789 from a mesoscale catchment using storage selection functions. *Water Resources Research*, 57, e2020WR028490.
790 <https://doi.org/10.1029/2020WR028490>

791 Nguyen, T. V., Kumar, R., Musolff, A., Lutz, S. R., Sarrazin, F., Attinger, S., & Fleckenstein, J. H. (2022). Disparate
792 seasonal nitrate export from nested heterogeneous subcatchments revealed with StorAge Selection functions. *Water*
793 *Resources Research*, 58, e2021WR030797. <https://doi.org/10.1029/2021WR030797>

794 Oldham, C. E., D. E. Farrow, and S. Peiffer (2013), A generalized damköhler number for classifying material
795 processing in hydrological systems, *Hydrology and Earth System Sciences*, 17(3), 1133–1148, doi:10.5194/hess-17-
796 1133-2013.

797 Pierce, F. J., Shaffer, M. J., Halvorson, A. D. 1991. Chapter 12: Screening procedure for estimating potentially
798 leachable nitrate-nitrogen below the root zone. *Managing Nitrogen for groundwater Quality and Farm Profitability*,
799 *Soil Science Society of America, USA*. pp.259-283

800 Rinaldo, A., P. Benettin, C. J. Harman, M. Hrachowitz, K. J. McGuire, Y. Van Der Velde, E. Bertuzzo, and G. Botter
801 (2015), Storage selection functions: A coherent framework for quantifying how catchments store and release water
802 and solutes, *Water Resources Research*, 51(6), 4840–4847.

803 Rivett, M. O., Buss, S. R., Morgan, P., Smith, J. W. N., & Bement, C. D. (2008). Nitrate attenuation in groundwater:
804 A review of biogeochemical controlling processes. *Water Research*, 42(16), 4215–4232.
805 <https://doi.org/10.1016/j.watres.2008.07.020>

806 Rodriguez, N. B., McGuire, K. J., & Klaus, J. (2018), Time-varying storage-water age relationships in a catchment
807 with a mediterranean climate. *Water Resources Research*, 54(6), 3988–4008.

808 Sayama, T. & McDonnell, J. J. (2009), A new time-space accounting scheme to predict stream water residence time
809 and hydrograph source components at the watershed scale. *Wat. Resour. Res.* 45, W07401.

810 Seibert, J., Grabs, T., Köhler, S., Laudon, H., Winterdahl, M., and Bishop, K.: Linking soil- and stream-water
811 chemistry based on a Riparian Flow-Concentration Integration Model, *Hydrol. Earth Syst. Sci.*, 13, 2287–2297,
812 <https://doi.org/10.5194/hess-13-2287-2009>, 2009.

813 Sprenger, M., Seeger, S., Blume, T., & Weiler, M. (2016), Travel times in the vadose zone: Variability in space and
814 time. *Water Resources Research*, 52, 5727–5754.

815 Therrien, R., McLaren, Sudicky, R. E., & Panday, S. (2010). *Hydrogeosphere: A three-dimensional numerical model*
816 *describing fully-integrated subsurface and surface flow and solute transport*, Groundwater Simulations Group.
817 Waterloo, ON: University of Waterloo.

818 Shaffer, M. J., Halvorson, A. D., Pierce, F. J. 1991. Chapter 13: Nitrate leaching and economic analysis package
819 NLEAP: model description and application. Managing Nitrogen for groundwater Quality and Farm Profitability, Soil
820 Science Society of America, USA. pp.285-322

821 Smith, R. L., Böhlke, J. K., Garabedian, S. P., Revesz, K. M., & Yoshinari, T. (2004). Assessing denitrification in
822 groundwater using natural gradient tracer tests with ^{15}N : In situ measurement of a sequential multistep reaction. *Water*
823 *Resources Research*, 40, W07101. [https:// doi.org/10.1029/2003WR002919](https://doi.org/10.1029/2003WR002919).

824 Stewart, M. K., Morgenstern, U. & McDonnell, J. J. (2010), Truncation of stream residence time: how the use of stable
825 isotopes has skewed our concept of streamwater age and origin. *Hydrol. Process.* 24, 1646-1659.

826 van der Velde, Y., G. De Rooij, J. Rozemeijer, F. Van Geer, and H. Broers (2010), Nitrate response of a lowland
827 catchment: On the relation between stream concentration and travel time distribution dynamics, *Water Resources*
828 *Research*, 46(11).

829 Stevenson, F.J., 1995. *Humus chemistry: genesis, composition, reactions*, Second Edition, Wiley. *J Chem Educ.* doi:
830 10.1021/ed072pA93.6, ISBN: 978-0-471-59474-1, 512 pp.

831 van der Velde, Y., P. J. J. F. Torfs, S. E. A. T. M. van der Zee, and R. Uijlenhoet (2012), Quantifying catchment-scale
832 mixing and its effect on time-varying travel time distributions, *Water Resources Research*, 48(6), n/a–n/a,
833 doi:10.1029/2011WR011310, w06536.

834 Van Meter, K. J., N. B. Basu, and P. Van Cappellen (2017), Two centuries of nitrogen dynamics: Legacy sources and
835 sinks in the mississippi and susquehanna river basins, *Global Biogeochemical Cycles*, 31(1), 2–23,
836 doi:10.1002/2016GB005498.

837 Werner, A. D., and C. T. Simmons (2009), Impact of sea-level rise on seawater intrusion in coastal aquifers, *Ground*
838 *Water*, 47, 197-204.

839 Wilusz, D. C., Harman, C. J., & Ball, W. P. (2017). Sensitivity of catchment transit times to rainfall variability under
840 present and future climates. *Water Resources Research*, 53(12), 10231-10256.

841 Wijayantiati, Y., Budihardjo, K., Sakamoto Y., Setyandito, O. (2017). Topsoil N-budget model in orchard farming to
842 evaluate groundwater nitrate contamination. *IOP Conf. Series: Earth and Environmental Science* 109 (2017) 012034.
843 doi:10.1088/1755-1315/109/1/012034.

844 Yang, J., I. Heidbüchel, A. Musolff, F. Reinstorf, and J. H. Fleckenstein (2018), Exploring the dynamics of transit
845 times and subsurface mixing in a small agricultural catchment, *Water Resources Research*, 54(3), 2317–2335,
846 doi:10.1002/2017WR021896.

847 Yang, J., Heidbüchel, I., Musolff, A., Xie, Y., Lu, C.*, Fleckenstein, J.H. (2021). Using nitrate as a tracer to constrain
848 age selection preferences in catchments with strong seasonality, *Journal of Hydrology*, 603, 126889. doi:
849 <https://doi.org/10.1016/j.jhydrol.2021.126889>.

850 Yang, J. (2022). DS2022-1YJ, HydroShare,
851 <http://www.hydroshare.org/resource/e266298e55834617a26242f6af9687e1>

852 Yang, X., Jomaa, S., & Rode, M. (2019). Sensitivity analysis of fully distributed parameterization reveals insights
853 into heterogeneous catchment responses for water quality modelling. *Water Resources Research*, 55, 10935–10953.
854 <https://doi.org/10.1029/2019WR025575>.

855 Yang, X., Jomaa, S., Zink, M., Fleckenstein, J. H., Borchardt, D., & Rode, M. (2018). A new fully distributed model
856 of nitrate transport and removal at catchment scale. *Water Resources Research*, 54, 5856–5877.
857 <https://doi.org/10.1029/2017WR022380>.

858 Zarlenga, A., & Fiori, A. (2020). Physically based modelling of water age at the hillslope scale: The Boussinesq age
859 equations. *HYDROLOGICAL PROCESSES*, 34(12), 2694-2706.

860 Zarlenga, A., Fiori, A., & Cvetkovic, V. (2022). On the interplay between hillslope and drainage network flow
861 dynamics in the catchment travel time distribution. *HYDROLOGICAL PROCESSES*, 36(3) [10.1002/hyp.14530].

862 Zhi, W., L. Li, W. Dong, W. Brown, J. Kaye, C. Steefel, and K. H. Williams (2019), Distinct source water chemistry
863 shapes contrasting concentration-discharge patterns, *Water Resources Research*, 55(5), 4233–4251,
864 doi:10.1029/2018WR024257.